

# *Tailoring viscoelastic properties of dynamic supramolecular poly(butadiene)-based elastomers*

Article

Published Version

Creative Commons: Attribution 4.0 (CC-BY)

Open Access

Hyder, M., O'Donnell, A. D., Chippindale, A. M. ORCID: <https://orcid.org/0000-0002-5918-8701>, German, I. M., Harries, J. L., Shebanova, O., Hamley, I. W. ORCID: <https://orcid.org/0000-0002-4549-0926> and Hayes, W. ORCID: <https://orcid.org/0000-0003-0047-2991> (2022) Tailoring viscoelastic properties of dynamic supramolecular poly(butadiene)-based elastomers. *Materials Today Chemistry*, 26. 101008. ISSN 2468-5194 doi: <https://doi.org/10.1016/j.mtchem.2022.101008> Available at <https://centaur.reading.ac.uk/105283/>

It is advisable to refer to the publisher's version if you intend to cite from the work. See [Guidance on citing](#).

To link to this article DOI: <http://dx.doi.org/10.1016/j.mtchem.2022.101008>

Publisher: Elsevier

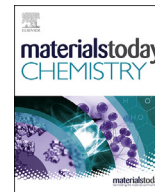
All outputs in CentAUR are protected by Intellectual Property Rights law, including copyright law. Copyright and IPR is retained by the creators or other copyright holders. Terms and conditions for use of this material are defined in the [End User Agreement](#).

[www.reading.ac.uk/centaur](http://www.reading.ac.uk/centaur)

**CentAUR**

Central Archive at the University of Reading

Reading's research outputs online



## Tailoring viscoelastic properties of dynamic supramolecular poly(butadiene)-based elastomers<sup>☆</sup>

M. Hyder<sup>a</sup>, A.D. O'Donnell<sup>a</sup>, A.M. Chippindale<sup>a</sup>, I.M. German<sup>b</sup>, J.L. Harries<sup>c</sup>,  
O. Shebanova<sup>d</sup>, I.W. Hamley<sup>a</sup>, W. Hayes<sup>a,\*</sup>

<sup>a</sup> Department of Chemistry, University of Reading, Whiteknights, Reading, RG6 6DX, UK

<sup>b</sup> Kinectrics Inc., 17-18 Frederick Sanger Road, The Surrey Research Park, Guildford, Surrey, GU2 7YD, UK

<sup>c</sup> Domino UK Ltd, Trafalgar Way, Bar Hill, Cambridge, CB23 8TU, UK

<sup>d</sup> Diamond Light Source, Diamond Light Source Ltd, Harwell Science & Innovation Campus, Didcot, OX11 0DE, UK



### ARTICLE INFO

#### Article history:

Received 7 April 2022

Received in revised form

20 May 2022

Accepted 24 May 2022

Available online 23 June 2022

#### Keywords:

Supramolecular materials

Healable

Adhesive

End-group control

### ABSTRACT

The discovery and development of new adhesive materials is critical for real-world applications of polymeric composite materials. Herein, we report the design and synthesis of a library of structurally related phase-separated supramolecular polyurethanes whose mechanical properties and adhesive characteristics can be enhanced through minor structural modifications of the polymer end-group. The interplay between phase separation of the hard domain polar end-groups and soft polybutadiene domains, coupled with tuneable self-assembly afforded by the polar end-groups, gives rise to a class of materials with tuneable mechanical properties. Exceptionally strong supramolecular adhesives and mechanically robust self-healing elastomers were identified. The mechanical properties were investigated through tensile testing. Finally, rheological analysis of the supramolecular materials was used to identify suitable healing and adhesive temperatures in addition to elucidate the supramolecular polyurethanes' thermal-responsive nature.

© 2022 The Author(s). Published by Elsevier Ltd. This is an open access article under the CC BY license (<http://creativecommons.org/licenses/by/4.0/>).

## 1. Introduction

Supramolecular materials offer many attractive properties, particularly durability, robustness, and performance. Many strategies have been employed to deliver supramolecular materials, ranging from host-guest interactions to complex supramolecular networks combining multiple orthogonal interactions [1–3]. In recent years, numerous polymers have been reported capable of self-healing upon exposure to a suitable stimulus [4–7]. Subsequently, supramolecular materials have seen application in adhesives [8–10], healable materials [11–16], inkjet and 3D printing [17,18], and biomedical applications [19–21].

Rowan, Weder and co-workers generated a tough optically healable supramolecular polymer through functionalisation of a soft telechelic poly(ethylene-co-butylene) with hard 2,6-bis(1'-methylbenzimidazolyl) pyridine ligands that assembled with

varying ratios of Zn(NTf<sub>2</sub>)<sub>2</sub> or La(NTf<sub>2</sub>)<sub>3</sub> [15]. The mechanical properties of the supramolecular polymer were attributed to phase separation between the hard and soft domains. To tailor the mechanical properties of supramolecular polymers, Schrettl and Weder combined two metallosupramolecular polymers, a rigid low molecular weight tri-functional semicrystalline polymer and a soft elastic telechelic polymer. Utilising the same metal-ligand complex as a binding motif, they found that by varying the ratio of the two constituents, they realised materials higher in ultimate tensile strength (UTS), modulus of toughness and elasticity than either supramolecular network in isolation [22]. Bouteiller and co-workers imparted self-healing properties to a PDMS thermoplastic elastomer by blending *n*-alkylated urea additives that can effectively soften the hard domains by accelerating the chain dynamics and disrupting bifurcated urea-urea stacking [23]. Meijer, Sijbesma and co-workers functionalised telechelic polymers, such as poly(ethylene-co-butylene)s [24] and polysiloxanes [25], with ureidopyrimidones (UPy) to deliver thermoreversible supramolecular materials. Anthamatten and co-workers integrated UPy side groups into linear and cross-linked siloxanes and realised biocompatible PDMS elastomers with control over variable

<sup>☆</sup> Dedicated to Professor Sir J. Fraser Stoddart F.R.S. on the occasion of his 80th birthday.

\* Corresponding author.

E-mail address: [w.c.hayes@reading.ac.uk](mailto:w.c.hayes@reading.ac.uk) (W. Hayes).

stiffness and viscoelastic relaxation [26]. Wilson and co-workers examined hydrogen-bonding motifs and created self-sorting networks [27,28].

Nitrophenyl urea motifs have found applications as supramolecular gelators, assembling through both urea-urea and urea-nitro interactions [29]. We have previously reported hydrogelator systems based on this motif [30,31], and their utility in creating polymer films capable of self-repair upon swelling [32]. Viscometry measurements performed by Bouteiller and co-workers highlighted the ability to enhance the hydrogen bonding capability of urea-based supramolecular systems by enforcing a non-coplanar conformation between the urea and the phenyl moiety, in turn enhancing hydrogen bonding [33]. Furthermore, we have recently demonstrated the influence of enhancing non-coplanar conformation between the urea and the phenyl moieties on hydrogelators systems [34].

Herein, we report the synthesis of a series of supramolecular polyurethanes (SPUs) in which attenuation of the assembly capabilities of the urea end-groups by conformational restriction, enforced by the presence of *ortho* substituents, has led to the ability to adjust the bulk properties of these materials. Through a better understanding of the urea-urea assembly and the disruptive capability of the nitro substituents, SPU materials with valuable properties, such as adhesion and healability, were afforded.

## 2. Experimental

### 2.1. Materials

Total Cray Valley kindly provided Krasol™ HLBH-P2000 for this study. Tetrahydrofuran (THF) was distilled from benzophenone and sodium before use. All other reagents were purchased from Sigma Aldrich and used as received. The synthesis and analysis of compounds **1–21** plus **SPU1–SPU13** are reported in the Supporting Information file.

### 2.2. Characterisation

$^1\text{H}$  NMR and  $^{13}\text{C}\{\text{H}\}$  NMR spectra were recorded on either a Bruker Nanobay 400 or a Bruker DPX 400 spectrometer operating at 400 MHz for  $^1\text{H}$  NMR or 100 MHz for  $^{13}\text{C}\{\text{H}\}$  NMR spectroscopic analysis. The data were processed using MestReNova Version 11.0.3–18688. Samples for NMR spectroscopic analysis were prepared in  $\text{CDCl}_3$ ,  $\text{DMSO}-d_6$  or  $d_8$ -THF, and dissolution of the sample was aided by gentle heating. Chemical shifts ( $\delta$ ) are reported in ppm relative to tetramethylsilane ( $\delta$  0.00 ppm) for  $\text{CDCl}_3$  and the residual solvent resonance ( $\delta$  2.50 ppm) for  $\text{DMSO}-d_6$  and ( $\delta$  1.73 ppm) for  $d_8$ -THF in  $^1\text{H}$  NMR. Infrared (IR) spectroscopic analysis was carried out using a Perkin Elmer 100 FT-IR (Fourier Transform Infrared) instrument with a diamond-ATR sampling accessory. Variable temperature IR (VT-IR) spectroscopic analysis was carried out using a Perkin Elmer 100 FT-IR spectrometer with a Specac variable temperature cell holder and Temperature Controller. The temperature was measured locally with a thermocouple embedded inside the solid cell frame. Mass spectrometry (MS) was conducted using a ThermoFisher Scientific Orbitrap XL LCMS. The sample was introduced by liquid chromatography (LC), and sample ionisation was achieved by electrospray ionisation (ESI). Melting points were recorded using a Stuart MP10 melting point apparatus and are uncorrected. An Agilent Technologies 1260 Infinity system was used to obtain gel permeation chromatography (GPC) analysis in HPLC-grade THF at a flow rate of 1.0 mL/min. Calibration was achieved using a series of near monodisperse polystyrene standards, and samples were prepared at a concentration of 1 mg/mL. Differential scanning calorimetry

measurements were performed on a TA Instruments DSC Q2000 adapted with a TA Refrigerated Cooling System 90, using aluminium TA Tzero pans and lids, measuring from  $-80$  °C to  $200$  °C with a heating and cooling rate of  $10$  °C  $\text{min}^{-1}$ . Thermogravimetric analysis (TGA) was carried out on TA Instruments TGA Q50 instrument with aluminium Tzero pans. The sample was heated from  $20$  °C to  $550$  °C at  $10$  °C  $\text{min}^{-1}$  under nitrogen gas with a flow rate of  $100$  mL/min. Rheological measurements were performed on a Malvern Panalytical Kinexus Lab + instrument fitted with a Peltier plate cartridge and 8 mm parallel plate geometry and analysed using rSpace Kinexus v1.76.2398 software. Tensile tests were carried out using a Thümler Z3-X1200 tensometer at a rate of  $10$  mm/min with a 1 KN load cell and THSSD-2019 software. The modulus of toughness was calculated by integrating the recorded plot to give the area under the curve. The trapezium rule was applied to calculate the area between zero strain to strain at break for each sample. The error reported is the standard deviation for the three repeats for each sample.

Small-angle X-ray scattering (SAXS) and Wide-angle X-ray scattering (WAXS) experiments were performed on beamline I22 at Diamond Light Source (Harwell, UK) [35]. Samples were mounted in modified DSC pans in a Linkam 600 DSC stage for temperature control. SAXS data were collected with a Pilatus 2 M detector and WAXS data with a Pilatus P3-2M detector. SAXS data were reduced using the software DAWN [36].

Crystals of **9**, **11–16**, **19**, and **21** were mounted under Paratone-N oil and flash cooled to  $100$  K under nitrogen in an Oxford Cryosystems Cryostream. Single-crystal X-ray intensity data were collected using a Rigaku XtaLAB Synergy diffractometer ( $\text{Cu } K\alpha$  radiation ( $\lambda = 1.54184$  Å)). The data were reduced within the Cry-SAlisPro software [37]. The structures were solved using the program Superflip [38], and all non-hydrogen atoms were located. Least-squares refinement against  $F$  was carried out using the CRYSTALS suite of programs [39]. The non-hydrogen atoms were refined anisotropically. All the hydrogen atoms were located in difference Fourier maps. The positions of the hydrogen atoms attached to nitrogen were refined with a  $U_{\text{iso}}$  of  $\sim 1.2$ – $1.5$  times the value of  $U_{\text{eq}}$  of the parent N atom. The hydrogen atoms attached to carbon were placed geometrically with a C–H distance of  $0.95$  Å and a  $U_{\text{iso}}$  of  $\sim 1.2$ – $1.5$  times the value of  $U_{\text{eq}}$  of the parent C atom, and the positions refined with riding constraints.

## 3. Results and discussion

The SPUs were designed to take advantage of multiple, complementary supramolecular interactions (see Fig. 1).  $\pi$ - $\pi$  stacking interactions derive from the choice of isocyanate, namely, methylene diphenyl diisocyanate (MDI). Other interactions result from urea bifurcated hydrogen bonds on the chain end, urethane hydrogen bonding in the polymer mid-block and urea-nitro hydrogen bonds between polymer chains. The position of the nitro-substituent was varied between the *-meta* and *-para* position, as previously we have shown that the two regioisomers behave very differently [31,32] and provide scope for optimisation of the mechanical properties of SPUs. Furthermore, the influence of steric bulk was investigated by employing methyl substituents placed at strategic substitution patterns probing the effect of conformationally controlling the end-group to tailor the mechanical properties of the resultant SPU.

A series of 13 aniline-derived end-cap groups were selected, incorporating *meta*-/*para*-nitro substitution and varying degrees of steric hindrance from methyl substituents on the aromatic ring. The synthetic routes used to access the four anilines not available commercially are shown in Scheme 1. In the case of anilines **1**, **2**, and **3**, which feature a nitro *-meta* to the amine unit, these were

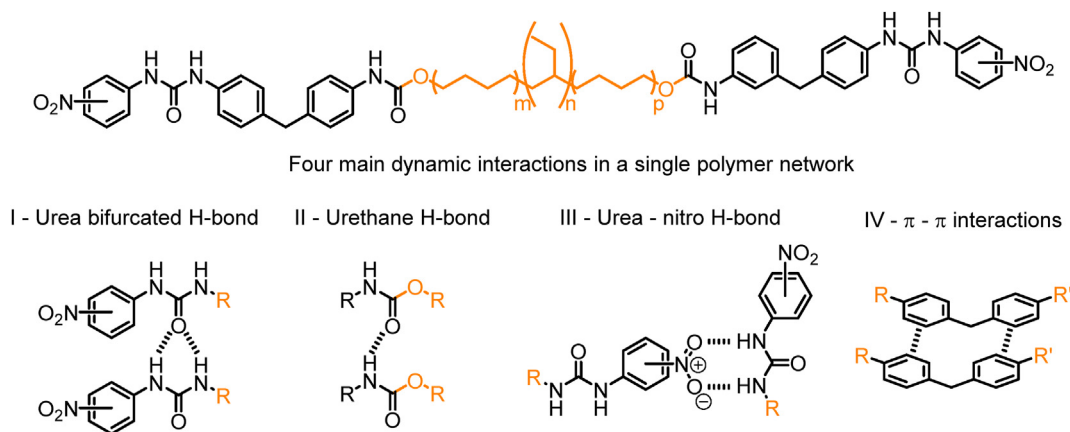
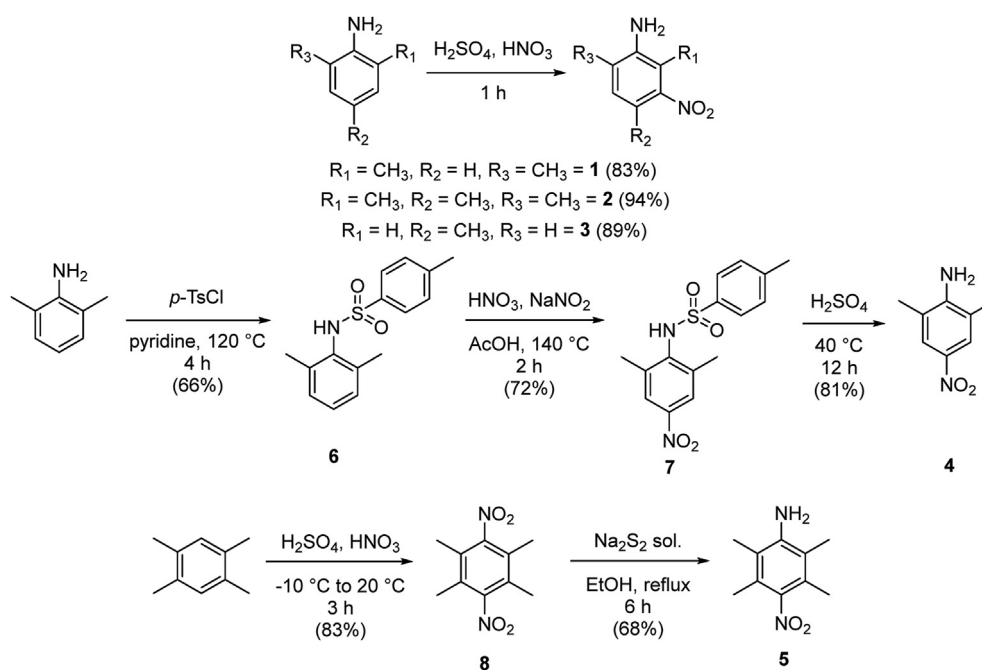


Fig. 1. Chemical structure and the four main dynamic bonds present in the SPUs synthesised in this study.



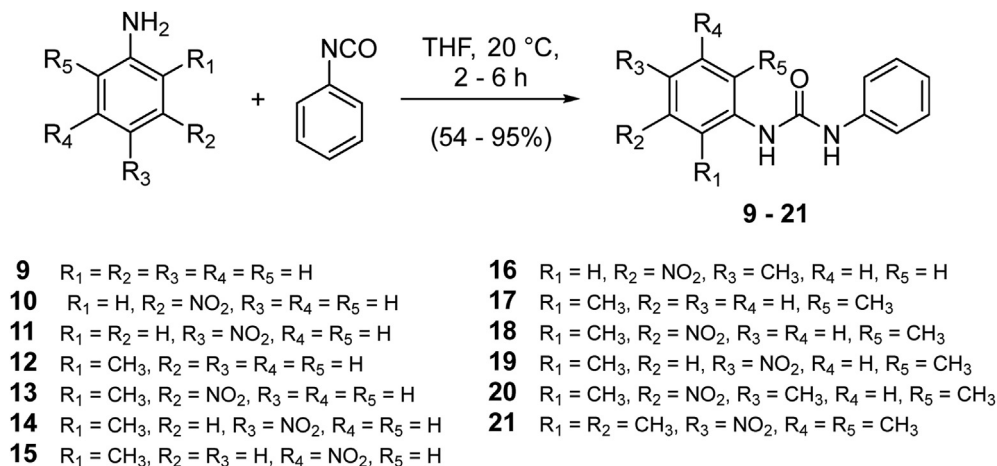
Scheme 1. The synthetic protocol for the synthesis of compounds 1–8 to afford the desired aniline derivatives: 2,6-dimethyl-3-nitroaniline **1**, 2,4,6-trimethyl-3-nitroaniline **2**, 4-methyl-3-nitroaniline **3**, 2,6-dimethyl-4-nitroaniline **4**, and 2,3,5,6-tetramethyl-4-nitroaniline **5** [34,41,42].

synthesised via the nitration of 2,6-xylidine [34], 2,4,6-trimethylaniline [40], and *p*-toluidine, respectively, to afford the desired compounds in good yield (83%, 94%, and 89%, respectively). More complex approaches were required to synthesise the *para*-nitro substituted **4** [34], and **5**. 2,6-Xylidine was first converted to the corresponding toluenesulfonamide **6** to promote nitration at the *para* position and the resulting *para*-nitro-toluenesulfonamide **7** was then treated with sulfuric acid to generate the desired 2,6-dimethyl-4-nitroaniline **4** in 81% yield. In the case of aniline **5**, 1,2,4,5-tetramethylbenzene was nitrated twice to form 1,2,4,5-tetramethyl-3,6-dinitrobenzene **7** and this was then selectively reduced by treatment with sodium disulfide to yield 2,3,5,6-tetramethyl-4-nitroaniline, **5**, in 68% yield [41]. The synthetic protocols for generating the compounds and polymers plus the associated analytical data are provided in the Supporting Information (SI) file (see Figs. S1–S68).

To understand how the spatial assembly of the supramolecular end-caps of **SPU1–SPU13** within the hard domains is affected by

the presence of *ortho*-methyl substituents adjacent to the urea and nitro moieties, a series of model bisaromatic ureas were synthesised, **9–21**. Ureas **9–21** were synthesised by reacting the respective aniline with phenyl isocyanate (see Scheme 2). The reactions were monitored by FTIR spectroscopy to observe the consumption of the isocyanate group,  $\nu_{\text{N}} = \text{C}=\text{O}_{(\text{stretch})}$  2275–2250  $\text{cm}^{-1}$ , and the formation of the corresponding urea,  $\nu_{\text{C}} = \text{O}_{(\text{stretch})}$  ca. 1640  $\text{cm}^{-1}$ . The solid-state geometries of the bisaromatic ureas and their hydrogen bonding patterns provide valuable insight into the assembly of **SPU1–SPU13**. Single crystals of the ureas **9**, **11–16**, **19** and **21** were grown via vapour diffusion or slow evaporation and studied by X-ray crystallography.

The key intermolecular interactions established from the X-ray analysis of the single crystals of ureas **9**, **11–16**, **19**, and **21** are shown in Fig. 2 (for the crystallographic data and detailed atom assignments, see Tables S1–S18 and Figs. S69–S77). The solid-state structures of compounds **9**, **11–16**, **19**, and **21** all reveal bifurcated hydrogen bonding between the urea carbonyl and the urea protons



**Scheme 2.** The general synthetic protocol used to afford the bisaromatic ureas **9–21** [43–46].

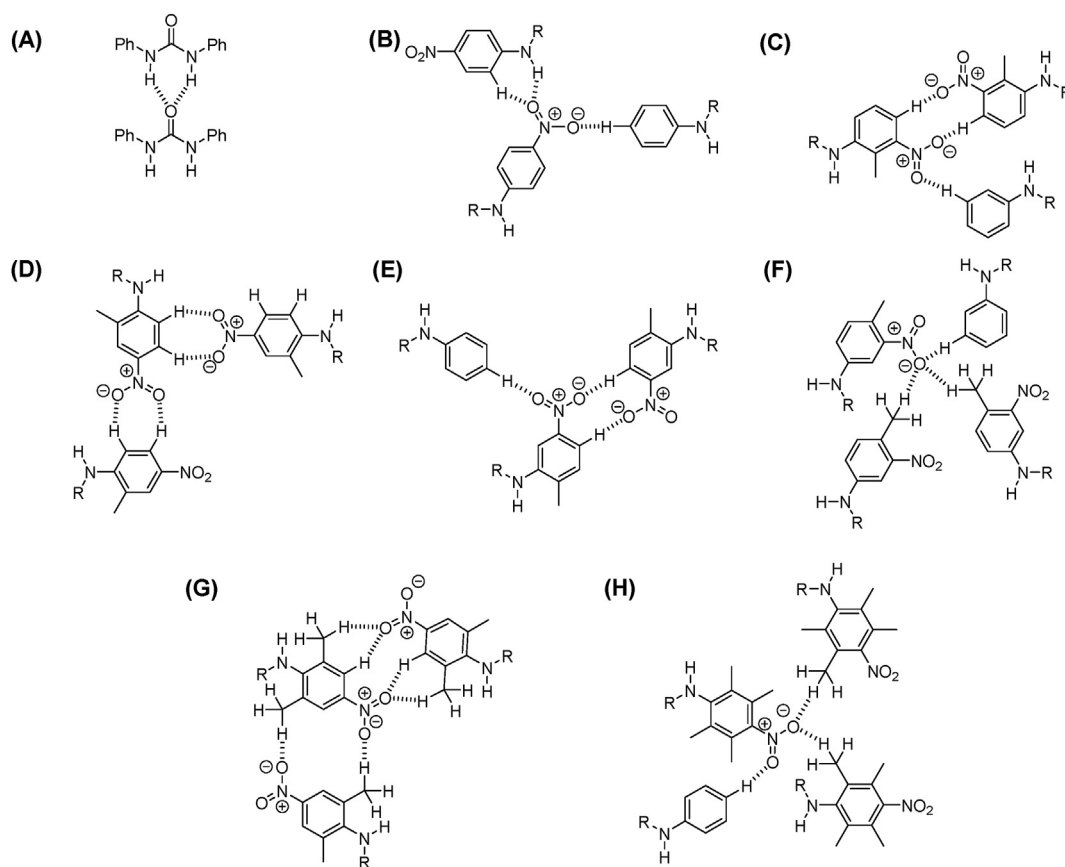


**Fig. 2.** Schematic representation of some of the hydrogen bonding motifs observed within the crystal structures of compounds **9**, **11**, **12**, **13**, **14**, **15**, **16**, **19**, and **21**. (A) Bifurcated urea-urea hydrogen bonding was observed in **9**, **11**, **12**, **13**, **14**, **15**, **16**, **19**, and **21**; (B) hydrogen bonding involving the nitro group observed in **11**; (C) hydrogen bonding of the nitro group observed in **13**; (D) hydrogen bonding observed in **14**; (E) hydrogen bonding involving the nitro group observed in **15**; (F) hydrogen bonding involving the nitro group observed in **16**; (G) hydrogen bonding involving the nitro group observed in **19**; (H) hydrogen bonding involving the nitro group observed in **21**.

of an adjacent molecule (Fig. 2A), with the singly methyl-substituted **12**, the *para*-nitro substituted **11**, **19**, and **21** and the *meta*-nitro substituted **13**, **15**, and **16**, exhibiting ordered 1-dimensional growth through this hydrogen-bonding motif. Urea **9**, which does not feature a nitro group [43], shows the strongest urea-urea hydrogen bonding with the shortest hydrogen bond lengths (O1 ··· H–N3: 2.131(18) Å; O1 ··· H–N10: 1.919(18) Å). On comparing **9** and **12**, the introduction of a single *ortho*-methyl

substituent increases the torsion angles from  $-38.1(2)^\circ$  and  $43.0(2)^\circ$  (for C2–N3–C4–C9 and C2–N10–C11–C12, respectively in **9**) to  $-45.7(2)^\circ$  and  $50.0(2)^\circ$  (for C2–N3–C4–C9 and C2–N10–C11–C16, respectively in **12**), with the latter torsion angle for **12** involving the *ortho*-methyl substituted ring. As observed in **12**, the presence of *ortho*-methyl substituents in **13**, **14** and **15** results in the substituted phenyl ring being twisted out of the plane to a greater degree compared to unsubstituted **11**, increasing the

torsion angle of C2–N10–C11–C16 from  $-28.3(3)^\circ$  (**11**) to  $-45.0(2)^\circ$  (**14**) and  $50.3(2)^\circ$  (**15**) and the C2–N3–C4–C5 torsion angle in **13** to  $62.9(4)^\circ$ . The introduction of two *ortho*-methyl substituents in **19** and **21** further twist the substituted phenyl ring out of the plane of the urea compared to the single *ortho*-methyl substituted **14**, increasing the torsion angle to  $-62.3(2)^\circ$  (C2–N3–C4–C12, **19**) and  $-78.1(4)^\circ$  (C2–N3–C4–C5, **21**). This twist results in stronger urea-urea hydrogen bonding in **13**, **14**, **15**, **19**, and **21**, as evidenced by their shorter hydrogen-bond lengths (O1  $\cdots$  H–N3: 2.082(44) Å; O1  $\cdots$  H–N14: 2.121(43) Å, **13**), (O1  $\cdots$  H–N3: 2.029(18) Å; O1  $\cdots$  H–N10: 2.167(18) Å, **14**), (O1  $\cdots$  H–N3: 2.151(20) Å; O1  $\cdots$  H–N10: 2.067(18) Å, **15**), (O1  $\cdots$  H–N3: 2.014(20) Å; O1  $\cdots$  H–N15: 2.087(20) Å, **19**), and (O1  $\cdots$  H–N3: 1.965(37) Å; O1  $\cdots$  H–N17: 2.051(39) Å, **21**), compared to those in **11** (O1  $\cdots$  H–N3: 2.045(20) Å; O1  $\cdots$  H–N10: 2.302(20) Å). As seen with the urea moiety, the incorporation of two methyl substituents *ortho* to the nitro, **21**, result in the nitro being twisted out of the plane of the substituted aryl ring, evident in the increase of the torsion angles of C11–C7–N8–O9 and C11–C7–N8–O10 from  $179.3(2)^\circ$  and  $0.0(3)^\circ$  (**11**),  $170.6(1)^\circ$  and  $-8.7(2)^\circ$  (**14**), and  $-175.2(1)^\circ$  and  $4.7(2)^\circ$  (**19**) to  $105.5(4)^\circ$  and  $-76.2(4)^\circ$  (**21**) respectively. This phenomena is also observed to a lesser extent with **13** and **16**, which only have a single methyl substituent *ortho* to the nitro, with an increase in torsion angles from  $176.8(1)^\circ$  and  $-3.1(2)^\circ$  (C14–C15–N17–O18 and C14–C15–N17–O19, respectively, **15**) to  $-31.4(5)^\circ$  and  $149.1(3)^\circ$  (C5–C6–N7–O8 and C5–C6–N7–O9, respectively, **13**), and  $-24.6(3)^\circ$  and  $150.5(2)^\circ$  (C7–C8–N10–O11 and C7–C8–N10–O12, respectively, **16**). Moving the methyl substituent from the *ortho*, **13**, to the *para*, **16**, position removes the steric hindrance experienced by the urea increasing the urea-urea hydrogen bond strength, evident in the shorter bond distances (O1  $\cdots$  H–N3: 2.082(44) Å; O1  $\cdots$  H–N14: 2.121(43) Å, **13**) and (O1  $\cdots$  H–N3: 2.091(21) Å; O1  $\cdots$  H–N14: 2.082(26) Å, **16**).

Additional, weaker intermolecular hydrogen bonds are observed in **11**, **13**–**16**, **19**, and **21**, with the nitro substituents as the acceptor moieties, as shown in Fig. 2. Hydrogen bonding mediated by the nitro group in **11**, as depicted in Fig. 2B, comprises one of the oxygen atoms of nitro behaving as an acceptor for both the NH donor and *ortho*-Ph hydrogen donor of the same molecule (O18  $\cdots$  H–N10: 2.65(2) Å; O18  $\cdots$  H–C12: 2.402(2) Å) and the other oxygen atom as an acceptor for a *para*-Ph hydrogen donor of an adjacent molecule (O19  $\cdots$  H–C7: 2.696(3) Å). A symmetrical hydrogen bonding arrangement in **13** (Fig. 2C) is observed between O9 of the nitro moiety and the *para*-Ph hydrogen donor on the substituted aryl ring of an adjacent molecule (O9  $\cdots$  H–C10: 2.667(4) Å). Further, the O9 atom of the nitro group acts as an acceptor for the *meta*-Ph hydrogen donor on the non-substituted aryl ring of an adjacent molecule (O8  $\cdots$  H–C19: 2.528(4) Å). The hydrogen bonding motif of the nitro group in **14** (Fig. 2D) consists of one oxygen atom behaving as the acceptor for the *ortho*-Ph hydrogen donor and the other oxygen as the acceptor for the *meta*-Ph hydrogen donor of the same molecule (O18  $\cdots$  H–C16: 2.583(2) Å and O19  $\cdots$  H–C15: 2.582(2) Å, respectively). The urea oxygen in **14** also acts as a weak acceptor for the *meta*-Ph hydrogen donor on the non-substituted phenyl ring (O1  $\cdots$  H–C8: 2.674(2) Å) (not shown). In **15** (Fig. 2E), one oxygen of the nitro moiety, O19, acts as an acceptor for the *para*-Ph hydrogen donor of an adjacent molecule. Further, the O19 atom of the nitro group of this adjacent molecule is an acceptor for the *para*-Ph hydrogen donor in the original molecule to form a symmetrical arrangement (O19  $\cdots$  H–C14: 2.535(2) Å). The second oxygen of the nitro group acts as an acceptor for the *para*-Ph hydrogen donor of the non-substituted phenyl ring of a separate molecule (O18  $\cdots$  H–C7: 2.585(2) Å). The nitro hydrogen bonding in **16**, (Fig. 2F), consists of O12 acting as an acceptor for two *para*-methyl donors on separate molecules, (O12  $\cdots$  H–C13:

2.599(3) Å; O12  $\cdots$  H–C13: 2.562(3) Å), as well as an acceptor for the *meta*-Ph donor on the unsubstituted aryl ring of a third molecule (O12  $\cdots$  H–C17: 2.689(2) Å). The hydrogen bonding in **19** (Fig. 2G), consists of two symmetrical arrangements, the first of which consists of O10 of the nitro moiety acting as an acceptor for the *meta*-Ph hydrogen donor and *ortho*-methyl hydrogen donor of an adjacent molecule which in turn forms a symmetrical arrangement (O10  $\cdots$  H–C11: 2.486(2) Å and O10  $\cdots$  H–C13: 2.690(2) Å). The second oxygen, O9, of the nitro group acts as an acceptor for the *ortho*-methyl hydrogen donor of a separate molecule which forms a second symmetrical arrangement (O9  $\cdots$  H–C14: 2.651(2) Å) [47]. In **21** (Fig. 2H), one oxygen of the nitro moiety, O10, acts as an acceptor for the *para*-Ph hydrogen donor of the non-substituted phenyl ring of a separate molecule (O10  $\cdots$  H–C21: 2.597(4) Å). The second oxygen of the nitro moiety, O9, acts as an acceptor for two methyl hydrogen donors on separate molecules one *ortho*-methyl and one *meta*-methyl (O9  $\cdots$  H–C13: 2.704(4) Å and O9  $\cdots$  H–C14: 2.586(5) Å, respectively). All of the solid state structures reveal  $\pi$ - $\pi$  interactions, with T-shaped interactions exhibited in compounds **9**, **11**, **16**, and **21** and displaced parallel  $\pi$ - $\pi$  interactions exhibited in **11**, **12**, **13**, **14**, **15**, **19**, and **21**.

The SPUs, **SPU1**–**SPU13**, were synthesised using the two-step process [48] (see Fig. 3A) that we previously used to generate supramolecular materials capable of healing at body temperature [49]. Briefly, Krasol™ HLBH-P2000 was reacted in bulk with 2.05 equivalents of MDI at 80 °C for 3 h to afford an isocyanate-terminated prepolymer. Each reaction vessel was then cooled to room temperature, solvated with THF, and 2.05 equivalents of end-cap were added before being brought to and maintained under reflux to furnish dynamic supramolecular materials (**SPU1**–**SPU13**). Each reaction was monitored by FTIR spectroscopy, and upon the disappearance of the isocyanate band, the polymers were then purified by repeated precipitations. Polymer films were subsequently solvent cast from a concentrated solution of THF, and the influence of modifying the end-group of the supramolecular polyurethane could then be assessed through mechanical property testing. Unwanted chain extension of the polyurethanes was minimal [48], and  $^1\text{H}$  NMR spectroscopic analysis revealed a ratio of 1:1 for the resonances associated with the urethanes and urea end-groups, which is consistent with the feed ratios (see the NMR spectroscopic data in the SI, Figs. S43–S68). The synthesis of the SPUs was first confirmed by  $^1\text{H}$  NMR spectroscopy which revealed resonances *ca.* 8.50 ppm and *ca.* 7.80 ppm, corresponding to the urethane protons in the prepolymer core and the urea protons of the aniline derivative end-caps, respectively.  $^{13}\text{C}$  NMR spectroscopy was also used to confirm the formation of the urethane and urea linkages, *ca.* 153 and 155 ppm, respectively. FTIR spectroscopic analysis of the polymers revealed the complete consumption of isocyanate functionalities, as noted by the disappearance of the isocyanate stretching absorption at  $2250$ – $2275\text{ cm}^{-1}$ . Additionally, the new absorbances observed at  $1640$ – $1680\text{ cm}^{-1}$  and  $1710$ – $1740\text{ cm}^{-1}$  were attributed to the newly formed urea/urethane moieties. GPC analysis of the polymers (See Figs. S78–90 and Table S19) was employed to confirm the degree of chain extension in the polyurethane, with an average of 3.5 hydrogenated poly(*n*-butadiene) residues per supramolecular polymer ( $M_n = 8700\text{ g/mol}$ ).

Quantitative analysis of both urethane and urea stretching vibrations observed in the FTIR spectra of **SPU1**–**SPU13** was conducted to calculate the degree of hydrogen bonding [50] and illustrate the effects of each end-cap on their respective polymer's supramolecular hydrogen-bonding network at 20 °C. The carbonyl stretching vibrations for hydrogen-bonded ( $1710\text{ cm}^{-1}$ ) and free ( $1740\text{ cm}^{-1}$ ) urethane groups were observed for all polymers, **SPU1**–**SPU13**, arising from the urethane linker bonds within the

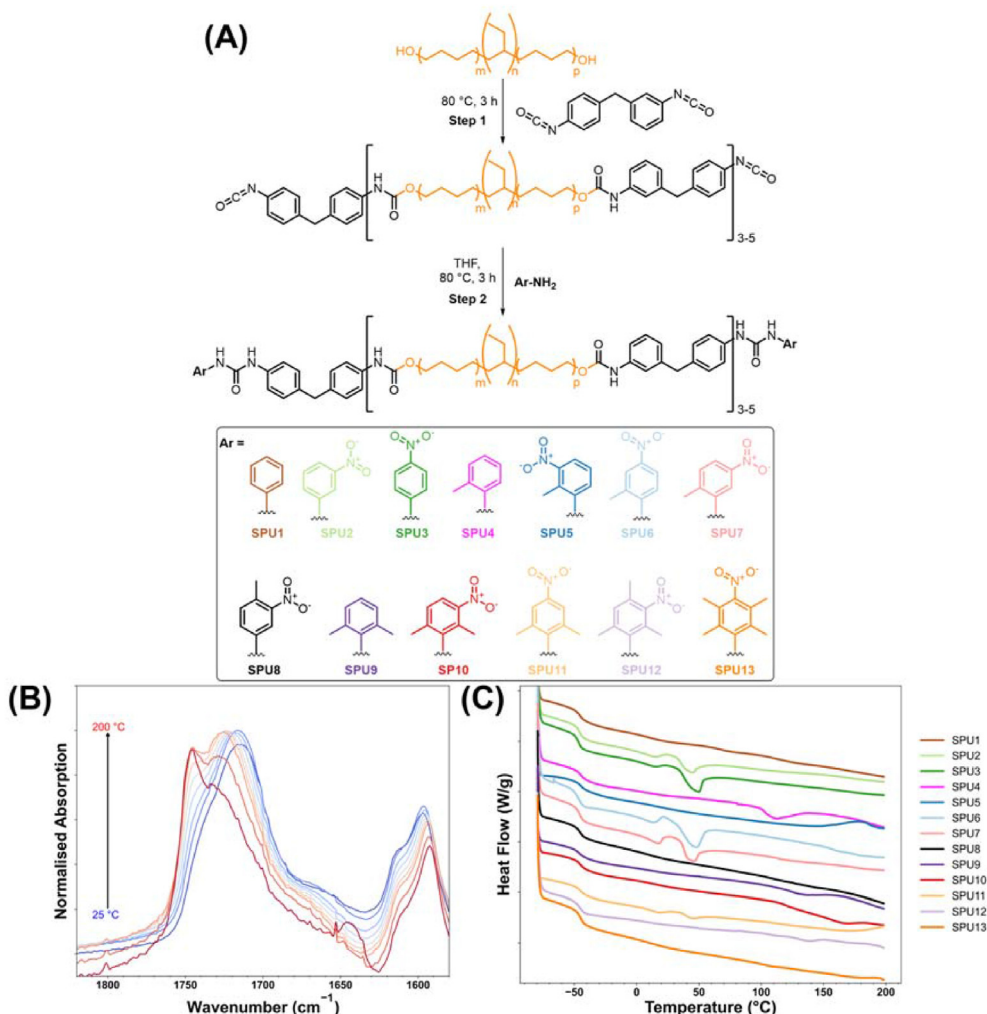


**Fig. 3.** (A) The synthetic strategy employed to synthesise supramolecular polymer networks SPU1–SPU13; (B) *In situ* VTIR spectra of SPU5 upon heating from 25 °C to 200 °C; (C) Stacked DSC plot of SPU1–SPU13 from the 2<sup>nd</sup> heating cycle.

polymer core [50]. The observation of the urea carbonyl stretching vibrations associated with the ordered hydrogen-bonded ( $1640\text{ cm}^{-1}$ ), disordered hydrogen-bonded ( $1656\text{--}1680\text{ cm}^{-1}$ ), and free ( $1692\text{ cm}^{-1}$ ) urea groups varied for polymers **SPU1**–**SPU13**; these stretching vibrations arise from the urea linker bonds formed by the polymer end-groups [51]. The degree of hydrogen

bonding within the supramolecular polymer networks was calculated by deconvoluting the carbonyl absorption bands from the FT-IR spectroscopic data (see Table 1 and Figs. S91–S104) [25]. Deconvolution of the urethane absorbances for the free and hydrogen-bonded carbonyls of **SPU1**–**SPU13** show a range of percentage hydrogen bonding, with **SPU1** exhibiting the lowest

**Table 1**

Normalised percentage integrals of the urethane and urea absorbances of **SPU1**–**SPU13** from their respective FT-IR spectra, where the total bound urea is equal to the sum of the ordered bound urea and disordered bound urea.

End-group	Bound Urethane (%)	Free Urethane (%)	Ordered Bound Urea (%)	Disordered Bound Urea (%)	Total Bound Urea (%)	Free Urea (%)
<b>SPU1</b>	64 ± 2	36 ± 6	50 ± 2	31 ± 4	81 ± 3	19 ± 5
<b>SPU2</b>	86 ± 3	14 ± 5	–	42 ± 4	42 ± 4	58 ± 3
<b>SPU3</b>	76 ± 2	25 ± 4	–	27 ± 4	27 ± 4	73 ± 2
<b>SPU4</b>	76 ± 3	25 ± 6	78 ± 2	14 ± 7	92 ± 3	8 ± 6
<b>SPU5</b>	80 ± 2	21 ± 3	49 ± 2	18 ± 6	67 ± 3	33 ± 5
<b>SPU6</b>	74 ± 2	26 ± 4	–	17 ± 6	17 ± 6	83 ± 3
<b>SPU7</b>	70 ± 2	30 ± 3	–	23 ± 5	23 ± 5	77 ± 2
<b>SPU8</b>	89 ± 6	11 ± 6	71 ± 2	13 ± 3	84 ± 2	16 ± 6
<b>SPU9</b>	78 ± 6	22 ± 4	71 ± 2	13 ± 5	85 ± 2	15 ± 5
<b>SPU10</b>	65 ± 2	35 ± 4	21 ± 5	26 ± 8	47 ± 7	53 ± 3
<b>SPU11</b>	70 ± 2	30 ± 5	31 ± 8	15 ± 8	46 ± 8	54 ± 5
<b>SPU12</b>	70 ± 2	30 ± 8	49 ± 4	27 ± 4	77 ± 4	23 ± 7
<b>SPU13</b>	81 ± 2	19 ± 4	56 ± 2	20 ± 6	76 ± 3	24 ± 6

percentage of hydrogen bonding ( $64 \pm 2\%$ ) and **SPU8** exhibiting the highest ( $89 \pm 6\%$ ), respectively. Unsurprisingly, changing the end-group had little discernible influence on the percentages of bound and unbound urethane carbonyls (see Figs. S91–S99). However, deconvolution of the urea-bound and unbound carbonyl absorbances provided vital insights into the supramolecular assembly in the solid state. Deconvolution of the carbonyl bands in their respective infrared spectra provided critical insight into the supramolecular assembly of the end-group (see Figs. S91–S105) [33,52,53]. In the absence of the nitro substituent, the influence of increasing the conformational restraint of the urea carbonyl into a non-coplanar arrangement with the aryl ring can be assessed. The *ortho*-methyl substituents on **SPU9** and **SPU4** increased the hydrogen-bonded urea, ordered and disordered, from  $81 \pm 3\%$  in **SPU1** to  $85 \pm 2\%$  and  $92 \pm 3\%$ , respectively. Interestingly, **SPU1**, which has no conformational restraint, was found to have  $81 \pm 3\%$  hydrogen-bonded urea, only  $50 \pm 2\%$  of which is ordered, the remaining  $31 \pm 4\%$  being disordered hydrogen bonding. **SPU9** and **SPU4** possessed  $71 \pm 2\%$  and  $78 \pm 2\%$  ordered hydrogen-bonded urea. Therefore, imparting the non-coplanar arrangement increases the ordered hydrogen bonding of the urea carbonyl and, as a result, encourages the  $\pi$ - $\pi$  stacking of the aryl moiety [33]. Interestingly the *ortho*-dimethyl substituted **SPU9** has fewer ordered hydrogen-bonded and overall hydrogen-bonded urea carbonyl groups than the *ortho*-methyl substituted **SPU4**, suggesting the increased steric hindrance around the urea moiety negatively affects the urea carbonyl group's ability to form ordered hydrogen bonds. The presence of a nitro moiety either *meta* (**SPU2**, **SPU5**, **SPU7**, **SPU8**, **SPU10**, and **SPU12**) or *para* (**SPU3**, **SPU6**, **SPU11**, and **SPU13**) to the urea on the aryl substituent has a dramatic influence on the degree and order of the urea-carbonyl hydrogen bonding, because of the introduction of a competitive hydrogen-bond acceptor which effectively disrupts urea-urea hydrogen bonding interactions in favour of urea-nitro interactions [54]. It is known that introducing nitro substitution of aryl ureas at either the *meta* or *para* position can drastically alter the 3-dimensional supramolecular assembly [31,55]. The introduction of the competitive nitro hydrogen bonding acceptors in **SPU2** and **SPU3**, where the nitro is *meta* and *para*, respectively, results in the absence of any ordered hydrogen-bonded urea carbonyl and a significant decrease in the percentage of hydrogen-bonded urea to  $42 \pm 4\%$  and  $27 \pm 4\%$ , respectively, when compared to **SPU1**. Contrary to that observed with **SPU4**, imparting conformational restraint of the urea to force a non-coplanar conformation of the urea and aryl groups with the presence of a single *ortho*-methyl moiety, while keeping the nitro in the same plane as the aryl ring, decreases the percentage of hydrogen-bonded urea for **SPU6** and **SPU7**. Increased steric hindrance experienced by the urea carbonyl further promotes the urea-nitro hydrogen bonding over urea-urea hydrogen bonding [33]. The *ortho*-methyl substituent adjacent to both the urea and nitro moieties in **SPU5** forces a non-coplanar conformation of both the urea and nitro with respect to the benzene ring. This non-coplanar conformation inhibits its resonance forms [41,56] which then inhibits its efficacy as a hydrogen-bond acceptor because of poor *p*-orbital overlap. This, along with the steric hindrance experienced by the nitro from the *ortho*-methyl, translates to  $49 \pm 2\%$  ordered hydrogen-bonded urea in **SPU5**. As observed with **SPU9**, the increase in the steric hindrance of the urea moiety the *ortho*-dimethyl substituted **SPU10** experiences compared to **SPU5** results in a decrease in overall hydrogen-bonded urea and ordered hydrogen-bonded urea. The opposite trend was observed when the nitro group was located in the *para* position and not hindered by an *ortho*-methyl substituent: in **SPU11**, an increase in both overall hydrogen-bonded urea and ordered hydrogen-bonded urea was observed,  $46 \pm 8\%$  and  $31 \pm 8\%$ , respectively, when compared to

**SPU6**. The *para*-methyl substituent adjacent to the nitro moiety in **SPU8** forces a non-coplanar conformation of the nitro with the aryl ring without influencing the geometry between the urea and aryl ring. Inhibition of the resonance experienced by the nitro moiety translates to a significant increase in both overall hydrogen-bonded urea and ordered hydrogen-bonded urea,  $84 \pm 2\%$  and  $71 \pm 2\%$ , respectively. Inducing full conformational restraint of both the urea and nitro when in *meta*-nitro substituted, **SPU12**, and *para*-nitro substituted, **SPU13**, results in the highest percentage of hydrogen-bonded urea when the urea is in the presence of *ortho*-methyl substituents,  $77 \pm 4\%$ , and  $76 \pm 3\%$ , respectively, and percentage of ordered hydrogen-bonded urea,  $49 \pm 4\%$ , and  $56 \pm 2\%$ , respectively. This promotion of urea-urea hydrogen-bonding over urea-nitro hydrogen-bonding is a result of the combined effect of the non-coplanar conformation adopted by the urea and aryl groups and the increased steric hindrance experienced by the nitro moieties from the *ortho*-methyl substituents, which in turn inhibits resonance from the induced nitro-aryl non-coplanar conformation.

We have previously illustrated the value of utilising VT-IR spectra to assess the reversibility of hydrogen-bonding functional groups in supramolecular polyurethanes [50]. To further understand the reversible processes in **SPU5**, VT-IR spectroscopic analysis was recorded from  $25^\circ\text{C}$  to  $200^\circ\text{C}$ , monitoring the relative absorbances of the urea and urethane carbonyl groups to understand the thermal stability of the hydrogen-bonded supramolecular networks of the urethane and urea moieties (see Fig. 3B). **SPU5** was prepared as a KBr disc with a loading of 0.1% wt. to ensure homogeneity throughout the beam path over the temperature range. Dissociation of the hydrogen-bonding networks within the SPU was assessed by deconvolution of the urea and urethane absorbances as a function of temperature (see Figs. S106–S109). Variation between the deconvoluted FT-IR and VT-IR spectra of **SPU5** was attributed to measurement differences: the room temperature FT-IR spectra were obtained from a polymer film on an ATR accessory, whereas the variable-temperature measurements used KBr discs. Upon increasing temperature, a shift to longer wavenumbers was observed for both the urethane and urea carbonyls moving from a bound to an unbound state. Qualitative comparison of the deconvoluted absorbances assigned to the bound and unbound urethane carbonyl groups throughout the heating cycle has revealed two thermal regions of interest. The first was evident from  $40^\circ\text{C}$  to  $80^\circ\text{C}$ , where an initial decrease in the percentage bound urethane was clear, with a second decrease from  $100^\circ\text{C}$  to  $140^\circ\text{C}$ . The deconvolution of the urea carbonyl has also revealed two thermal regions of interest,  $40^\circ\text{C}$ – $60^\circ\text{C}$  and  $80^\circ\text{C}$  to  $120^\circ\text{C}$ . The first is associated with a transition from ordered bound urea to disordered bound urea, and the second region is attributed to a transition of the disordered bound urea to free urea. However, the complete dissociation of the hydrogen-bonded carbonyls was not evident up to  $200^\circ\text{C}$ .

The thermal properties of **SPU1**–**SPU13** were assessed by DSC analysis (see Fig. 3C and Table 2). In the second heating cycle, all the SPUs exhibited a  $T_g$  ca.  $-45^\circ\text{C}$  that was associated with the glass transition of the poly(ethylene-co-butylene) soft domain. **SPU5** displayed the thermal characteristics of a typical amorphous polymer in that only a single glass transition was evident. Interestingly, the SPUs which contained a nitro functional group that lay in-plane with the aryl ring, such as **SPU6**, exhibited two distinct melting transitions in the second heating run,  $13.4^\circ\text{C}$  and  $36.0^\circ\text{C}$ , and a cold crystallisation between these melting transitions at around  $16^\circ\text{C}$  and crystallisation was also evident in the first cooling cycle at  $23.1^\circ\text{C}$ . Apart from **SPU12**, which features an elevated melting temperature of  $124.0^\circ\text{C}$ , these data indicate that when the nitro substituent of the end-group is twisted orthogonal to the aryl ring by an *ortho* methyl substituent, the resultant SPUs do not have

**Table 2**  
Thermal properties of the supramolecular polymers SPU1–SPU13.

	$T_g$ (°C) <sup>b</sup>	$T_m$ (°C) <sup>a</sup>	$T_m$ (°C) <sup>b</sup>	$T_c$ (°C) <sup>c</sup>	$T_c$ (°C) <sup>b,d</sup>
<b>SPU1</b>	–45.7	98.9	–	–	–
<b>SPU2</b>	–45.6	41.0	13.7; 33.0	16.8	17.1
<b>SPU3</b>	–46.1	41.1	13.3; 34.2	22.8	16.5
<b>SPU4</b>	–44.5	56.1	–	–	–
<b>SPU5</b>	–45.0	–	–	–	–
<b>SPU6</b>	–46.1	40.7	13.4; 36.0	23.1	15.9
<b>SPU7</b>	–45.7	42.0	14.1; 35.7	22.1	18.9
<b>SPU8</b>	–45.5	–	–	–	–
<b>SPU9</b>	–46.3	–	15.0; 36.8	11.3	20.0
<b>SPU10</b>	–45.3	–	–	–	–
<b>SPU11</b>	–44.9	40.0	8.6; 36.3	16.2	19.6
<b>SPU12</b>	–45.9	42.3	124.0	–	–
<b>SPU13</b>	–44.6	–	–	–	–

<sup>a</sup> First heating run, 10 °C min<sup>–1</sup>.

<sup>b</sup> Second heating run, 10 °C min<sup>–1</sup>.

<sup>c</sup> First cooling run, 10 °C min<sup>–1</sup>.

<sup>d</sup> Cold crystallisation.

melting transitions that are discernible by DSC analysis. This trend was evident in the SPUs synthesised herein. As **SPU1–SPU13** all have similar molecular weights and polydispersity (see Table S19), the differences were seen in thermal transitions originate purely from the aggregation and crystallisation of the end-group in the hard domains. The melting and crystallisation of the hard domains are proposed to be a consequence of nanofiber formation, which Appel et al. have previously reported for ureidopyrimidinone supramolecular thermoplastic elastomers [57]. SAXS/WAXS experiments were therefore performed on the supramolecular polyurethane networks to further investigate the crystallinity within the hard domain in more detail.

TGA analysis was employed to ascertain the maximum processing temperature, whereby samples were heated from 20 °C to 550 °C at a rate of 10 °C min<sup>–1</sup> under a nitrogen atmosphere. **SPU13** exhibited the lowest temperature for the onset of degradation at 237 °C, and all the SPUs degraded fully by 475 °C (See Figs. S110–S115).

The properties of thermoplastic supramolecular polyurethanes are dependent on their microphase-separated morphology [58–60]. SAXS has thus been used to investigate the microphase separation in these materials [11,50,61]. At room temperature, **SPU2**, **SPU3**, **SPU6**, and **SPU10** exhibit broad Bragg peaks at 95.1 Å, 84.0 Å, 87.0 Å, and 82.7 Å, respectively, implying a microphase-separated morphology arising from the immiscibility of the hard hydrogen-bonding end-groups with the soft poly(butadiene) backbone [48,50,61,62]. In the cases of **SPU3** and **SPU6**, an *-ortho*-methyl substituent on the end-groups resulted in a clear shift to longer interdomain spacings from 84.0 Å to 87.0 Å. The most significant change, however, was observed in the case of **SPU2** and **SPU10**; in the absence of *-ortho*-methyl substituents, the interdomain spacing (**SPU2**) was 95.1 Å, and upon constraining the conformation of the end-cap through the addition of two *-ortho* methyl substituents, a significant shift to 82.7 Å was evident (see Fig. 4A). In the case of **SPU5**, where only one methyl substituent is *ortho* to the urea, and the nitro substituent is twisted out of plane relative to the aryl substituent, a broad Bragg peak was observed at 62.8 Å, indicating a reduced degree of microphase separation between the polymer backbone and the end-group. When compared to our previously reported supramolecular poly(butadiene)s, which featured chiral end-groups, broad reflections were observed with domain spacings of 101.3 Å and were associated with the nanophase separation [50]. **SPU1**, **SPU4**, and **SPU9** are end-capped with an aniline that does not feature the nitro hydrogen-bonding acceptor group and the difference in the SAXS data between

these SPUs and those SPUs where the end-groups possess a nitro moiety is dramatic. Bragg peaks associated with microphase separation are significantly less intense and are shifted to larger domain spacings, implying reduced microphase separation between the polar end-groups and the apolar polymer backbone. Furthermore, **SPU9** exhibited a second-order peak suggesting a lamellar structure.

WAXS was also performed to investigate the ordering within the hard domains (see Fig. 4B). Several reflections were observed (*ca.* 14.6 Å, 9.8 Å, 7.4 Å, 5.5 Å, 4.7 Å, 4.2 Å, 3.5 Å and 3.1 Å). All the SPUs in this study exhibited well-ordered packing with reflections (*ca.* 4.7 Å to 4.2 Å) corresponding to ordering within the urea based hard domains [63]. Furthermore, reflections (*ca.* 3.5 Å), characteristic of  $\pi$ – $\pi$  stacking assemblies, can be seen [64]. **SPU4** and **SPU9**, which do not contain a nitro substituent, feature sharp reflections, especially *ca.* 4.7 to 4.2 Å corresponding to urea-urea hydrogen-bonding interactions. Deconvolution of FTIR spectroscopic data revealed that these SPUs had the highest ordered urea hydrogen-bonding content (see Table 1).

Visual inspection of the polymer films provided critical insight into the assembly of the end-group. **SPU1**, **SPU4**, and **SPU9**, which did not feature a nitro substituent, did not form homogeneous films and instead appeared significantly phase-separated (see Fig. S116, a photograph of **SPU12** is also shown in Fig. S117). The viscoelastic properties of **SPU1–SPU13** were assessed with dynamic rheological testing (see Fig. 5A and 5B, Figs. S118–130). The storage modulus ( $G'$ ) dominates, and **SPU1–SPU13** behave as viscoelastic solids in the low-temperature regime. At elevated temperatures, the differences between **SPU1–SPU13** became apparent, and the dissociation and association of supramolecular polymer networks could be compared. The strong association of the hard domains in **SPU1**, **SPU4** and **SPU9** and lack of nitro substituent resulted in no meaningful change in the storage modulus up to 100 °C. This data reinforces the concept that the nitro substituent on the polymer end-group attenuates the interchain hydrogen bonding. A similar observation was made by Nicoud and co-workers who investigated nitrophenyl urea crystal structures and found that the nitro oxygen acts as a competitive acceptor for acidic urea hydrogen donors and disrupts urea-urea interactions [65]. In the case of **SPU1**, a gradual relaxation mechanism was observed, yet the polymer did not transition into the viscous state (see Fig. 5B). **SPU4** and **SPU9**, which feature *ortho*-methyl substituents, resist this relaxation mechanism, presumably because of the hard domains' increased association and crystallinity and hence increased order within the domain. **SPU2**, **SPU3**, **SPU6** and **SPU7** exhibited terminal flow below 60 °C and crossover between  $G'$  and the loss modulus ( $G''$ ) was observed. The common feature of these SPUs is that they all possess a nitro functional group and in the case of **SPU6** and **SPU7**, a single methyl substituent situated *ortho* to the urea moiety. Therefore, these SPUs were investigated for their potential as low-temperature adhesives and healable materials to exploit their reversible dissociation. Interestingly, **SPU5**, which also features a nitro substituent and an *ortho*-methyl substituent (to both the nitro and urea groups), exhibited exceptional resistance to temperature and no terminal flow nor significant relaxation event was observed up to 150 °C. In this case, the *ortho*-methyl substituent can twist the nitro group out of the plane of the aryl ring [56] and disrupt its ability to act as a hydrogen-bond acceptor and thus, **SPU5** exhibits similar rheological characteristics to **SPU1**, **SPU4** and **SPU9**. SPUs **SPU10**, **SPU11**, **SPU12** and **SPU13**, which contained two *ortho*-methyl substituents and therefore more organised hard domains, because of the forced non-coplanar assembly, also did not exhibit dramatic changes in their rheological properties with increasing temperature. **SPU11**, however, is the exception, as in this case, the nitro substituent is located in the *para* position and thus able to act

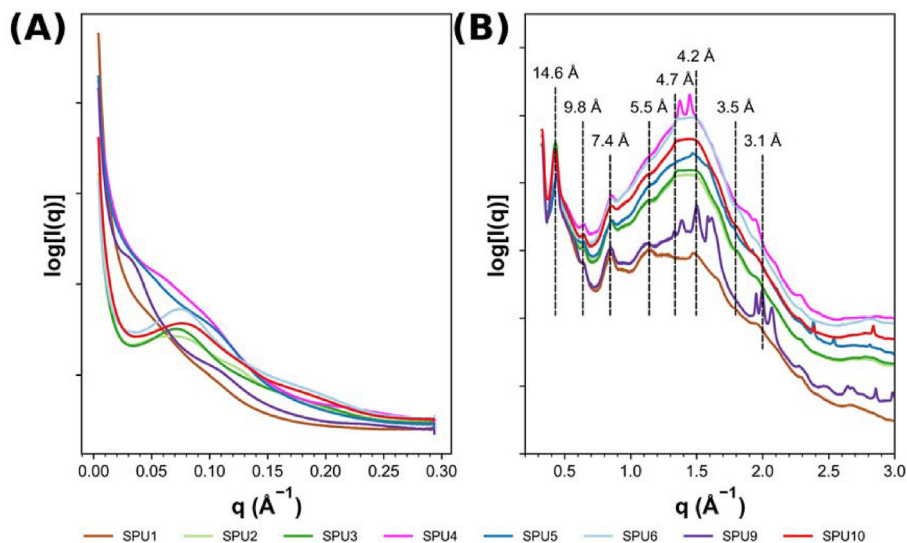


Fig. 4. (A) SAXS intensity profiles of the SPUs (B) WAXS intensity profiles of the SPUs. Data were acquired at room temperature.

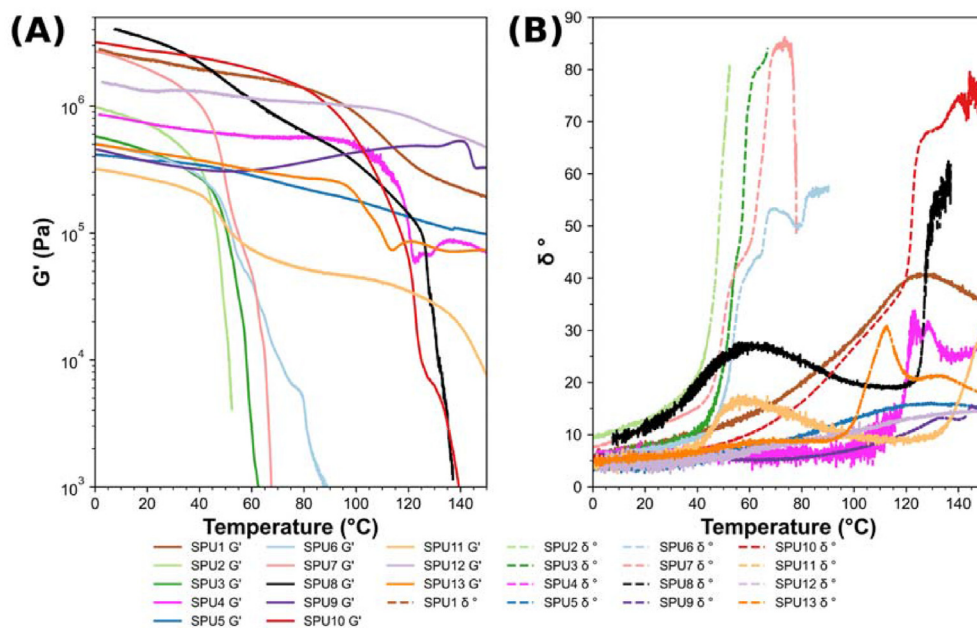


Fig. 5. Temperature sweep analysis of **SPU1–13** over a temperature regime of 0 °C–150 °C, using a normal force of 1 N and a frequency of 1 Hz. (A)  $G'$  against temperature, (B) phase shift ( $\delta$ ) against temperature.

as an uninhibited hydrogen-bonding acceptor, and a noticeable relaxation event is observed around 40 °C (see Fig. 5B), presumably softening of the hard domains, however, a new rubbery plateau is found. The supramolecular network can resist terminal flow up to 140 °C, where the onset of terminal flow is observed. As observed with **SPU11**, **SPU8** which contains a *para*-methyl adjacent to the nitro moiety experiences a significant relaxation event around 40 °C with a new rubbery plateau being found after, resisting terminal flow up to 120 °C. Master curves of  $G'$  and  $G''$  for **SPU2**, **SPU3**, **SPU5–SPU8** and **SPU10–SPU13** were attempted using the time-temperature superposition (TTS) principle; however, the frequency curves could not be fitted with only horizontal shift factors (see Figs. S131–S140). van Gurp-Palmen plots were used to confirm this (see Figs. S141–S150). The principle of TTS can at times fail in systems when there is more than one assembly mode with

distinctly different temperature dependencies, and this is observed commonly in immiscible polymer blends [66]. In our case, it is postulated that the four main dynamic hydrogen-bonding interactions involving these end-groups had distinctly different temperature dependencies and as such, we were unable to apply TTS for all of the SPUs tested.

We have demonstrated previously that the supramolecular assembly of nitro-aryl urea hydrogelators can be controlled by conformationally forcing the urea and aryl substituents into a non-coplanar arrangement [34]. Changing the end-group of the supramolecular polymer networks synthesised in this study significantly affected mechanical properties by changing the supramolecular-assembly mode. The binding interactions in the polar hard domains (e.g., the end-groups) dictates the supramolecular cross-link density and thus mechanical properties of the polymer network.

Tensile stress-strain measurements probed the mechanical properties of the supramolecular elastomers at a rate of 10 mm/min (Fig. 6).

The general structure of supramolecular polyurethanes and the four primary dynamic interactions give rise to their unique mechanical properties (see Fig. 1) (see Figs. S151–165). It is helpful to evaluate the *-meta* and *-para*-nitro supramolecular polyurethanes separately to assess and effectively discuss the differences in mechanical properties. The SPUs featuring each regioisomer behave differently, and the influence of the pattern of substituents surrounding the nitro substituent was critical. Assessing first the *meta*-nitro substituted supramolecular polyurethanes (SPU2, SPU5, SPU7, SPU8, SPU10, and SPU12), a drastic increase in both ultimate tensile strength (UTS) and Young's modulus was obtained in SPU12. In SPU12, where the end-group was 2,4,6-trimethyl-3-nitroaniline, a UTS of  $6.08 \pm 0.29$  MPa and Young's modulus of  $38.96 \pm 0.60$  MPa was achieved. This result was in contrast to that obtained for SPU10 (2,6-dimethyl-3-nitroaniline), which had the second-lowest UTS in

this study of  $1.22 \pm 0.01$  MPa and the second-lowest Young's modulus at  $5.22 \pm 0.14$  MPa. The only primary structural difference between these two supramolecular elastomers is the addition of a single methyl substituent that flanks the nitro substituent position, enforcing non-coplanarity between the nitro and the aryl ring. In contrast, when the end-group was 3-nitroaniline (SPU2), a UTS value of  $1.27 \pm 0.00$  MPa and Young's modulus of  $8.68 \pm 0.63$  MPa was determined comparable in value to SPU10. However, SPU10 proved to be the most elastic supramolecular polymer in this study, with an elongation at break (EB) of  $2.39 \pm 0.04$ . SPU5 offers a unique insight into how adding a single *-ortho*-methyl substituent adjacent to both the urea and nitro moieties resulted in more than doubling the UTS than compared to the cases of SPU2, SPU7, and SPU10. Rationalising this outcome is non-trivial, and the influence of the methyl substituent appears to be two-fold; when located *ortho* to the urea, the plane of the aryl unit is twisted into a non-coplanar arrangement; this effect is also magnified when two methyl substituents flank the urea group. Secondly, when a methyl

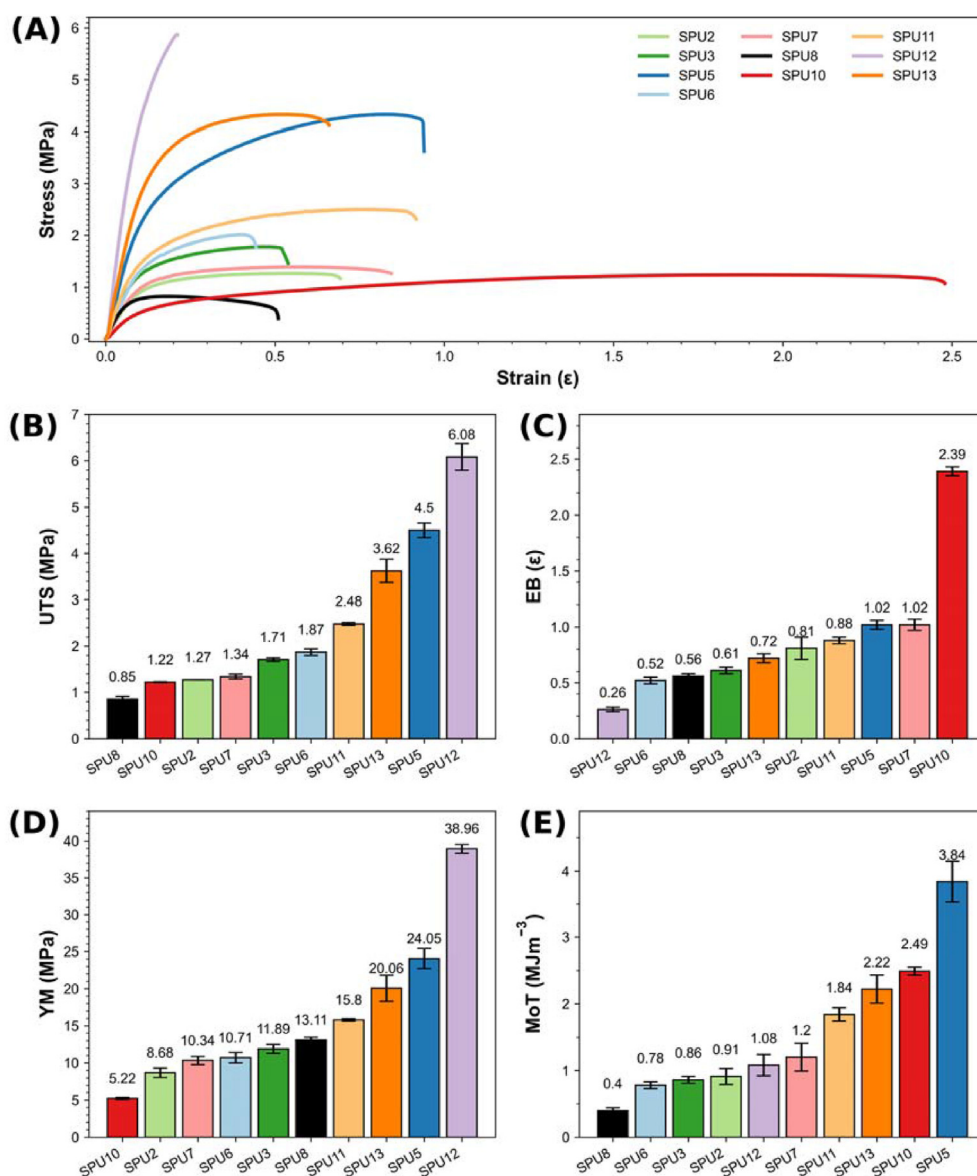


Fig. 6. (A) Representative stress-strain curves of supramolecular elastomers, SPU2, SPU3, SPU5–SPU7 and SPU10–SPU13. Comparison of (B) ultimate tensile strength (UTS), (C) elongation at break (EB), (D) Young's modulus, and (E) Modulus of toughness (MoT). The error shown is the standard deviation between the three repeats for each sample.

substituent is situated *-ortho* to the nitro substituent, the nitro acceptor unit can twist out-of-plane and act as a hydrogen bonding acceptor to adjacent polymer chains perpendicular to the main chain. To our surprise, having two methyl substituents flanking the urea (in the case of the end-group of **SPU10**) serves to affect the UTS of the SPU negatively. Evaluating the *-para* regioisomer (**SPU3**, **SPU6**, **SPU11**, and **SPU13**) and removing the influence of the *-ortho* methyl substituent, a trend appears, for all parameters tested. The difference between **SPU6** and **SPU3** is negligible, suggesting that the addition of a single methyl substituent *ortho* to the urea has no significant effect on the hard domain. This correlates to the absence of ordered hydrogen bonding of the urea carbonyl within the FT-IR spectroscopic analysis (see Table 1). However, in the case of **SPU11**, where two methyl substituents flank the urea and force non-coplanarity between the urea and the aryl substituent, marked increases in UTS, EB, Young's modulus, and modulus of toughness were observed (Fig. 6B-E). **SPU13** exemplifies this observation further, with the largest UTS, Young's modulus and modulus of toughness compared to the other *para*-nitro substituted SPUs (Table 3). These observations correlate to the introduction of ordered hydrogen-bonded urea carbonyls in the cases of **SPU11** and **SPU13**, with **SPU13** featuring the highest percentage of ordered and total hydrogen-bonded urea carbonyl within the *para*-nitro substituted SPUs (see Table 1).

Adhesion between two substrates requires strong interfacial interactions and is a non-trivial challenge. We envisaged that by taking advantage of the tuneable supramolecular assembly through end-group design, our supramolecular networks could more efficiently dissipate mechanical load by breaking physical (non-covalent) interactions and therefore reduce adhesive and cohesive failure. These non-covalent interactions will reform after breaking and restore the polymer adhesive's mechanical properties with sufficient time and temperature [22,67,68]. Advantageously, our relatively low molecular weight supramolecular polymer adhesives have the advantage of reversibility and derive their mechanical properties from non-covalent interactions. Consequently, they do not suffer the same mechanical property loss as polymer systems that rely on chain scission for energy dissipation. We tested the hot-melt adhesion properties of the supramolecular polymer networks through triplicate lap-shear experiments. The adhesion of the supramolecular polymers was assessed at two different bonding temperatures, 70 °C and 120 °C, to understand the bulk viscoelastic properties in more detail. Four substrates, namely, glass, aluminium, high-density polyethylene (HDPE) and polypropylene (PP) were assessed (Fig. 7A). Unsurprisingly, strong adhesion was achieved with glass (see Fig. S155) and aluminium substrates as the supramolecular polyurethanes can interact with the substrate through non-covalent interactions [69,70]. **SPU12** exhibited exceptional

shear strength in adhering to glass ( $5.70 \pm 0.10$  MPa) and aluminium ( $3.59 \pm 0.23$  MPa). To put this in context, Feringa, Tian and co-workers explored a thioctic acid copolymer with a maximum lap shear strength of 2.5 MPa when adhering glass, making it comparable to 3 M instant adhesive at 2.25 MPa [52]. Similarly, Weder and co-workers reported an optically responsive supramolecular polymer glass that took advantage of the self-assembly characteristics of UPy units. Adhesion of two glass slides bonded together by the supramolecular polymer glass yielded a lap shear strength of approximately 1.2 MPa [71]. To demonstrate the reusability of these SPUs as adhesives, re-adhesion of **SPU12** between glass substrates was conducted and exhibited no fatigue after 5 times of cycling (Fig. 7B), this observation is owing to the dynamic nature of supramolecular materials. In contrast, adhesion to HDPE and PP proved challenging, as these substrates do not have surface structural motifs that can cooperatively interact with the supramolecular polyurethanes. Hydrogen-bonding interactions are highly directional and must be within 5 Å of each other and be orientated cooperatively throughout the bulk material to be effective [72]. Thus, we anticipated controlling this bulk orientation through effective end-group modulation. Interestingly an inverse relationship was observed for **SPU7** whereby it was found to be the strongest adherent to PP with a shear strength of  $1.43 \pm 0.14$  MPa and surprisingly the weakest to HDPE ( $0.58 \pm 0.03$  MPa).

The polymer healing tests were conducted by first cutting the polymer tensile strips in half with a scalpel, and the edges were butted together on a PTFE plate [49]. The strips were then transferred into a preheated oven for 1 h at an appropriate temperature derived from the rheological data for each SPU before allowing to cool to room temperature for 30 min and carefully peeling from the PTFE plate (see Fig. S156, [73]). It has been previously reported that for a strong self-healing response, the relaxation time of the polymer film should range from 0.1 s to 100 s [74]. For this to occur,  $G'$  and  $G''$  need to crossover at the determined healing temperature. **SPU5** and **SPU11–SPU13** do not exhibit crossover between  $G'$  and  $G''$  at temperatures below 150 °C, as evident in the temperature sweep analysis (see Fig. 5) and TTS analysis (see Figs. S131–S150, respectively). As a result of the absence of material flow for these SPUs, poor recovery of mechanical properties was observed, and healing was not observed for **SPU12**. **SPU3**, **SPU6** and **SPU7** all exhibited modest recoveries, 53%, 53% and 39%, respectively, in terms of UTS and increases in their EB relative to the pristine material, 249%, 167% and 137% (Table 4). **SPU2** and **SPU10** saw an increase in their UTS (134% and 220%) and a modest recovery in EB (37% and 54%). Healing recoveries greater than 100% have been observed previously for other elastomer systems described by Bao, Binder and co-workers presumably a consequence of the preparation conditions used to afford the pristine material not permitting

**Table 3**

Effect of end-group on the mechanical properties of the SPUs; the recorded are averages of three separate samples of each SPU. The error shown is the standard deviation between the three repeats for each sample.

End-group	UTS <sup>a</sup> (MPa)	EB <sup>b</sup> (e)	Young's Modulus <sup>a</sup> (MPa)	Modulus of Toughness <sup>a</sup> (MJm <sup>-3</sup> )
<b>SPU2</b>	1.27 ± 0.00	0.81 ± 0.10	8.68 ± 0.63	0.91 ± 0.12
<b>SPU3</b>	1.71 ± 0.04	0.61 ± 0.03	11.89 ± 0.60	0.86 ± 0.05
<b>SPU5</b>	4.50 ± 0.16	1.02 ± 0.04	24.05 ± 1.33	3.84 ± 0.31
<b>SPU6</b>	1.87 ± 0.07	0.52 ± 0.03	10.71 ± 0.70	0.78 ± 0.05
<b>SPU7</b>	1.34 ± 0.05	1.02 ± 0.15	10.34 ± 0.55	1.20 ± 0.21
<b>SPU8</b>	0.85 ± 0.06	0.56 ± 0.02	13.11 ± 0.35	0.41 ± 0.04
<b>SPU10</b>	1.22 ± 0.01	2.39 ± 0.04	5.22 ± 0.14	2.49 ± 0.06
<b>SPU11</b>	2.48 ± 0.03	0.88 ± 0.03	15.80 ± 0.16	1.84 ± 0.10
<b>SPU12</b>	6.08 ± 0.29	0.26 ± 0.02	38.96 ± 0.60	1.08 ± 0.16
<b>SPU13</b>	3.62 ± 0.25	0.72 ± 0.04	20.06 ± 1.75	2.22 ± 0.21

<sup>a</sup> UTS, ultimate tensile strength.

<sup>b</sup> EB, elongation at break.

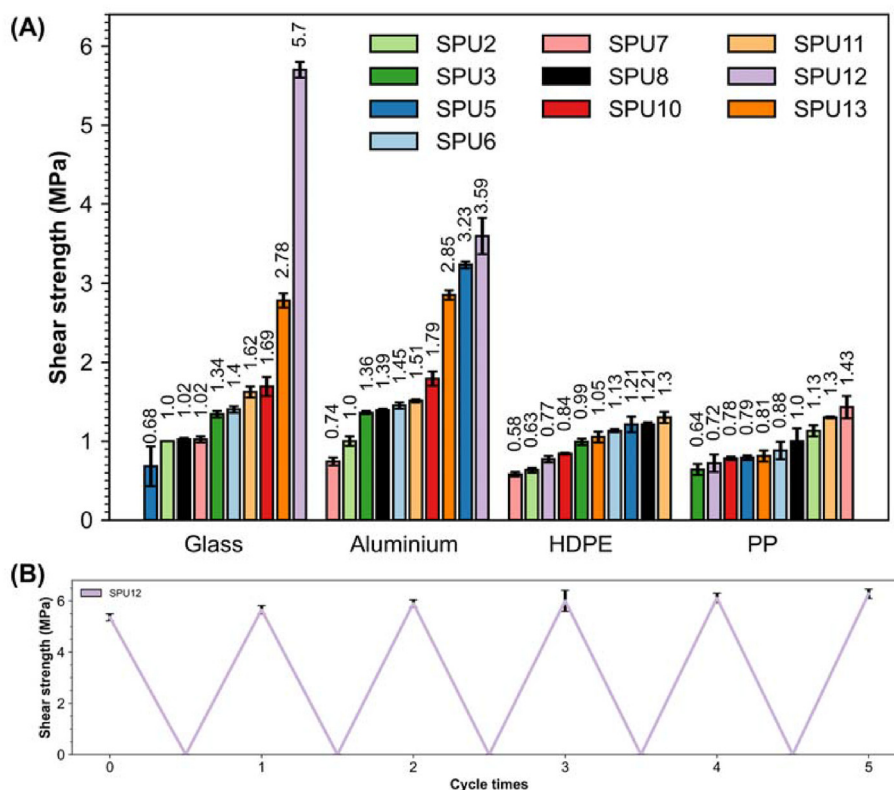


Fig. 7. A) Shear strength of supramolecular networks as determined by tensile lap-shear experiments. B) Shear strength of SPU after cycling 5 times cycling experiments.

Table 4

Healing data for the SPUs; the order of data in the table for each entry is as follows: pristine SPU; healed SPU; % healing.

End-group	Healed UTS (MPa)	Healed EB ( $\epsilon$ )	Healed Young's Modulus (MPa)	Healed Modulus of Toughness ( $\text{MJm}^{-3}$ )
SPU2	1.27 $\pm$ 0.00	0.81 $\pm$ 0.10	8.68 $\pm$ 0.63	0.91 $\pm$ 0.12
	1.70 $\pm$ 0.15	0.30 $\pm$ 0.04	13.68 $\pm$ 0.81	0.39 $\pm$ 0.09
	134%	37%	158%	43%
SPU3	1.71 $\pm$ 0.04	0.61 $\pm$ 0.03	11.89 $\pm$ 0.60	0.86 $\pm$ 0.05
	0.90 $\pm$ 0.06	1.52 $\pm$ 0.24	6.99 $\pm$ 0.95	1.17 $\pm$ 0.23
	53%	249%	59%	136%
SPU5	4.50 $\pm$ 0.16	1.02 $\pm$ 0.04	24.05 $\pm$ 1.33	3.84 $\pm$ 0.31
	1.36 $\pm$ 0.32	0.07 $\pm$ 0.02	28.50 $\pm$ 3.99	0.08 $\pm$ 0.03
	30%	7%	119%	2%
SPU6	1.87 $\pm$ 0.07	0.52 $\pm$ 0.03	10.71 $\pm$ 0.70	0.78 $\pm$ 0.05
	1.00 $\pm$ 0.06	0.87 $\pm$ 0.14	8.69 $\pm$ 0.57	0.67 $\pm$ 0.12
	53%	167%	81%	86%
SPU7	1.34 $\pm$ 0.05	1.02 $\pm$ 0.15	10.34 $\pm$ 0.55	1.20 $\pm$ 0.21
	0.52 $\pm$ 0.04	1.40 $\pm$ 0.32	4.84 $\pm$ 0.10	0.61 $\pm$ 0.16
	39%	137%	47%	51%
SPU8	0.85 $\pm$ 0.06	0.56 $\pm$ 0.02	13.11 $\pm$ 0.35	0.41 $\pm$ 0.04
	0.58 $\pm$ 0.00	0.41 $\pm$ 0.00	10.49 $\pm$ 1.63	0.19 $\pm$ 0.00
	68%	72%	80%	47%
SPU10	1.22 $\pm$ 0.01	2.39 $\pm$ 0.04	5.22 $\pm$ 0.14	2.49 $\pm$ 0.06
	2.68 $\pm$ 0.13	1.28 $\pm$ 0.14	9.94 $\pm$ 0.06	2.49 $\pm$ 0.42
	220%	54%	190%	100%
SPU11	2.48 $\pm$ 0.03	0.88 $\pm$ 0.03	15.80 $\pm$ 0.16	1.84 $\pm$ 0.10
	0.94 $\pm$ 0.09	0.47 $\pm$ 0.04	6.43 $\pm$ 0.42	0.32 $\pm$ 0.07
	38%	53%	41%	17%
SPU12	6.08 $\pm$ 0.29	0.26 $\pm$ 0.02	38.96 $\pm$ 0.60	1.08 $\pm$ 0.16
	–	–	–	–
	–	–	–	–
SPU13	3.62 $\pm$ 0.25	0.72 $\pm$ 0.04	20.06 $\pm$ 1.75	2.22 $\pm$ 0.21
	1.38 $\pm$ 0.40	0.24 $\pm$ 0.05	12.96 $\pm$ 1.89	0.22 $\pm$ 0.10
	38%	33%	65%	10%

the supramolecular networks in question to reach their energetic minimum [74].

#### 4. Conclusions

A series of novel SPUs that feature polar end-groups were synthesised, and their physical properties were assessed with respect to their end-groups. End-groups that did not feature a nitro moiety were too brittle and phase-separated because of increased crystallinity in the hard domain. Upon attenuating this assembly with a nitro substituent, which acted as a competitive hydrogen-bonding group for urea-urea associations, the mechanical properties of the resultant SPUs could be tailored and adhesion to glass, aluminium, PP and HDPE was assessed. Furthermore, these SPU derivatives were also found to be elastomeric and self-healing. SAXS/WAXS analysis revealed a microphase separated morphology which was attributed to the improved mechanical properties of the SPUs. DSC analysis showed that SPUs with unhindered nitro substituents exhibited melt transitions centred around 36 °C. Temperature sweep rheological analysis of the SPUs revealed key insights, into the reversibility of the supramolecular networks, in the absence of a nitro substituent crossover between  $G'$  and  $G''$  was not observed. This was also the case when the nitro substituent was twisted out of plane relative to the aryl ring and therefore unable to act as a competitive hydrogen bonding acceptor.

#### Credit author statement

**Matthew Hyder:** Conceptualisation, Validation, Formal analysis, Investigation, Writing - Original Draft. **Adam D. O'Donnell:** Conceptualisation, Formal analysis, Investigation, Writing - Original Draft, Visualization, Supervision. **Ann M. Chippindale:** Formal analysis & Editing. **Ian M. German:** Writing - Review & Editing, Supervision. **Josephine L. Harries:** Writing - Review & Editing, Supervision. **Olga Shebanova:** Investigation. **Ian W. Hamley:** Formal analysis, Editing & Funding acquisition for beamtime (ref. SM22909) **Wayne Hayes:** Conceptualisation, Resources, Writing - Review & Editing, Supervision, Project administration, Funding acquisition.

#### Data availability

The raw/processed data required to reproduce these findings cannot be shared at this time due to technical or time limitations.

#### Declaration of competing interest

The authors declare that they have no known competing financial interests or personal relationships that could have appeared to influence the work reported in this paper.

#### Acknowledgements

The authors would like to acknowledge financial support from the University of Reading and Domino Printing Sciences Ltd (PhD studentship for MH) and EPSRC and Kinectrics UK Ltd (PhD studentship for ADOD). In addition, the University of Reading (EPSRC-Doctoral Training Grant) is acknowledged for providing access to instrumentation in the Chemical Analysis Facility. We thank Cray Valley for supplying Krasol™ HLBH-P2000, Mr Nick Spencer (University of Reading) for his help in collecting the single-crystal X-ray diffraction data and Miss Jemma Harding for her contributions in support of the research. We thank Diamond for the award of beamtime, ref. SM22909.

#### Appendix A. Supplementary data

Supplementary data to this article can be found online at <https://doi.org/10.1016/j.mtchem.2022.101008>.

#### References

- [1] T.F.A. de Greef, E.W. Meijer, Supramolecular polymers, *Nature* 453 (2008) 171–173, <https://doi.org/10.1038/453171a>.
- [2] J.-M. Lehn, Perspectives in chemistry-aspects of adaptive chemistry and materials, *Angew. Chemie Int. Ed.* 54 (2015) 3276–3289, <https://doi.org/10.1002/anie.201409399>.
- [3] F. Huang, O.A. Scherman, Supramolecular polymers, *Chem. Soc. Rev.* 41 (2012) 5879–5880, <https://doi.org/10.1039/c2cs90071h>.
- [4] M.W. Urban, Stratification, stimuli-responsiveness, self-healing, and signaling in polymer networks, *Prog. Polym. Sci.* 34 (2009) 679–687, <https://doi.org/10.1016/j.progpolymsci.2009.03.004>.
- [5] J. Li, J.A. Viveros, M.H. Wrue, M. Anthamatten, Shape-memory effects in polymer networks containing reversibly associating side-groups, *Adv. Mater.* 19 (2007) 2851–2855, <https://doi.org/10.1002/adma.200602260>.
- [6] J.T. Kim, B.K. Kim, E.Y. Kim, S.H. Kwon, H.M. Jeong, Synthesis and properties of near IR induced self-healable polyurethane/graphene nanocomposites, *Eur. Polym. J.* 49 (2013) 3889–3896, <https://doi.org/10.1016/j.eurpolymj.2013.10.009>.
- [7] C. Heinzmann, S. Coulibaly, A. Roulin, G.L. Fiore, C. Weder, Light-induced bonding and debonding with supramolecular adhesives, *ACS Appl. Mater. Interfaces* 6 (2014) 4713–4719, <https://doi.org/10.1021/am405302z>.
- [8] X. Ji, M. Ahmed, L. Long, N.M. Khashab, F. Huang, J.L. Sessler, Adhesive supramolecular polymeric materials constructed from macrocycle-based host-guest interactions, *Chem. Soc. Rev.* 48 (2019) 2682–2697, <https://doi.org/10.1039/c8cs00955d>.
- [9] J. Courtois, I. Baroudi, N. Nouvel, E. Degrandi, S. Pensec, G. Ducouret, C. Chanéac, L. Bouteiller, C. Creton, Supramolecular soft adhesive materials, *Adv. Funct. Mater.* 20 (2010) 1803–1811, <https://doi.org/10.1002/adfm.200901903>.
- [10] J. Liu, C.S.Y. Tan, O.A. Scherman, Dynamic interfacial adhesion through cucurbit[n]uril molecular recognition, *Angew. Chemie - Int. Ed.* 57 (2018) 8854–8858, <https://doi.org/10.1002/anie.201800775>.
- [11] S. Burattini, B.W. Greenland, D.H. Merino, W. Weng, J. Seppala, H.M. Colquhoun, W. Hayes, M.E. MacKay, I.W. Hamley, S.J. Rowan, A healable supramolecular polymer blend based on aromatic  $\pi$ - $\pi$  Stacking and hydrogen-bonding interactions, *J. Am. Chem. Soc.* 132 (2010) 12051–12058, <https://doi.org/10.1021/ja104446r>.
- [12] L.R. Hart, J.L. Harries, B.W. Greenland, H.M. Colquhoun, W. Hayes, Healable supramolecular polymers, *Polym. Chem.* 4 (2013) 4860–4870, <https://doi.org/10.1039/c3py00081h>.
- [13] L.R. Hart, J.H. Hunter, N.A. Nguyen, J.L. Harries, B.W. Greenland, M.E. Mackay, H.M. Colquhoun, W. Hayes, Multivalency in healable supramolecular polymers: the effect of supramolecular cross-link density on the mechanical properties and healing of non-covalent polymer networks, *Polym. Chem.* 5 (2014) 3680–3688, <https://doi.org/10.1039/c4py00292j>.
- [14] S. Coulibaly, A. Roulin, S. Balog, M.V. Biyani, E.J. Foster, S.J. Rowan, G.L. Fiore, C. Weder, Reinforcement of optically healable supramolecular polymers with cellulose nanocrystals, *Macromolecules* 47 (2014) 152–160, <https://doi.org/10.1021/ma402143c>.
- [15] M. Burnworth, L. Tang, J.R. Kumpfer, A.J. Duncan, F.L. Beyer, G.L. Fiore, S.J. Rowan, C. Weder, Optically healable supramolecular polymers, *Nature* 472 (2011) 334–337, <https://doi.org/10.1038/nature09963>.
- [16] P. Cordier, F. Tournilhac, C. Soulié-Ziakovic, L. Leibler, Self-healing and thermoreversible rubber from supramolecular assembly, *Nature* 451 (2008) 977–980, <https://doi.org/10.1038/nature06669>.
- [17] L.R. Hart, J.L. Harries, B.W. Greenland, H.M. Colquhoun, W. Hayes, Molecular design of a discrete chain-folding polyimide for controlled inkjet deposition of supramolecular polymers, *Polym. Chem.* 6 (2015) 7342–7352, <https://doi.org/10.1039/c5py00622h>.
- [18] L.R. Hart, S. Li, C. Sturgess, R. Wildman, J.R. Jones, W. Hayes, 3D printing of biocompatible supramolecular polymers and their composites, *ACS Appl. Mater. Interfaces* 8 (2016) 3115–3122, <https://doi.org/10.1021/acsami.5b10471>.
- [19] Z. Wang, M. Shui, I.W. Wyman, Q.W. Zhang, R. Wang, Cucurbit[8]uril-based supramolecular hydrogels for biomedical applications, *RSC Med. Chem.* 12 (2021) 722–729, <https://doi.org/10.1039/d1md00019e>.
- [20] H. Jin, W. Huang, X. Zhu, Y. Zhou, D. Yan, Biocompatible or biodegradable hyperbranched polymers: from self-assembly to cytomimetic applications, *Chem. Soc. Rev.* 41 (2012) 5986–5997, <https://doi.org/10.1039/c2cs35130g>.
- [21] A.W. Bosman, P.Y.W. Dankers, H.M. Janssen, E.W. Meijer, G.M.L. van Gemert, *Modular Supramolecular Materials for Biomedical Uses*, 2008. WO 2007/058539 A2.
- [22] J. Sautaux, F. Marx, I. Gunkel, C. Weder, S. Schrettl, Mechanically robust supramolecular polymer co-assemblies, *Nat. Commun.* 13 (2022) 1–9, <https://doi.org/10.1038/s41467-022-28017-0>.
- [23] L. Simonin, G. Falco, S. Pensec, F. Dalmas, J.M. Chenal, F. Ganachaud, A. Marcellan, L. Chazeau, L. Bouteiller, Macromolecular additives to turn a

- thermoplastic elastomer into a self-healing material, *Macromolecules* 54 (2021) 888–895, <https://doi.org/10.1021/acs.macromol.0c02352>.
- [24] B.J.B. Folmer, R.P. Sijbesma, R.M. Versteegen, J.A.J. van der Rijt, E.W. Meijer, Supramolecular polymer materials: chain extension of telechelic polymers using a reactive hydrogen-bonding synthon, *Adv. Mater.* 12 (2000) 874–878, <https://doi.org/10.1002/1521-4095.200006>; 12:12<874>:AID-ADMA874>3.0.CO;2-C.
- [25] J.H.K.K. Hirschberg, F.H. Beijer, H.A. van Aert, P.C.M.M. Magusin, R.P. Sijbesma, E.W. Meijer, Supramolecular polymers from linear telechelic siloxanes with quadruple-hydrogen-bonded units, *Macromolecules* 32 (1999) 2696–2705, <https://doi.org/10.1021/ma981950w>.
- [26] Y. Meng, W. Xu, M.R. Newman, D.S.W. Benoit, M. Anthamatten, Thermoreversible siloxane networks: soft biomaterials with widely tunable viscoelasticity, *Adv. Funct. Mater.* 29 (2019) 1–9, <https://doi.org/10.1002/adfm.201903721>.
- [27] M.L. Pellizzaro, K.A. Houton, A.J. Wilson, Sequential and phototriggered supramolecular self-sorting cascades using hydrogen-bonded motifs, *Chem. Sci.* 4 (2013) 1825–1829, <https://doi.org/10.1039/c3sc22194f>.
- [28] H.M. Coubrough, S.C.C. van der Lubbe, K. Hetherington, A. Minard, C. Pask, M.J. Howard, C. Fonseca Guerra, A.J. Wilson, Supramolecular self-sorting networks using hydrogen-bonding motifs, *Chem. Eur. J.* 25 (2019) 785–795, <https://doi.org/10.1002/chem.201804791>.
- [29] F. Piana, D.H. Case, S.M. Ramalhet, G. Pileio, M. Facciotti, G.M. Day, Y.Z. Khimyak, J. Angulo, R.C.D. Brown, P.A. Gale, Substituent interference on supramolecular assembly in urea gelators: synthesis, structure prediction and NMR, *Soft Matter* 12 (2016) 4034–4043, <https://doi.org/10.1039/c6sm00607h>.
- [30] F. Rodríguez-Llansola, B. Escuder, J.F. Miravet, D. Hermida-Merino, I.W. Hamley, C.J. Cardin, W. Hayes, Selective and highly efficient dye scavenging by a pH-responsive molecular hydrogelator, *Chem. Commun.* 46 (2010) 7960–7962, <https://doi.org/10.1039/c0cc02338h>.
- [31] D.M. Wood, B.W. Greenland, A.L. Acton, F. Rodríguez-Llansola, C.A. Murray, C.J. Cardin, J.F. Miravet, B. Escuder, I.W. Hamley, W. Hayes, pH-tunable hydrogelators for water purification: structural optimisation and evaluation, *Chem. Eur. J.* 18 (2012) 2692–2699, <https://doi.org/10.1002/chem.201102137>.
- [32] B.C. Baker, I.M. German, A.M. Chippindale, C.E.A.A. McEwan, G.C. Stevens, H.M. Colquhoun, W. Hayes, Nitroarylurea-terminated supramolecular polymers that exhibit facile thermal repair and aqueous swelling-induced sealing of defects, *Polymer* 140 (2018) 1–9, <https://doi.org/10.1016/j.polymer.2018.02.029>.
- [33] B. Isare, G. Pembouong, F. Boué, L. Bouteiller, Conformational control of hydrogen-bonded aromatic bis-ureas, *Langmuir* 28 (2012) 7535–7541, <https://doi.org/10.1021/la300887p>.
- [34] A.D. O'Donnell, A.G. Gavriel, W. Christie, A.M. Chippindale, I.M. German, W. Hayes, Conformational control of bis-urea self-assembled supramolecular pH switchable low-molecular-weight hydrogelators, *Arkivoc* 2021 (2021) 222–241, <https://doi.org/10.24820/ark.5550190.p011.581>.
- [35] A.J. Smith, S.G. Alcock, L.S. Davidson, J.H. Emmins, J.C. Hiller Bardsley, P. Holloway, M. Malfois, A.R. Marshall, C.L. Pizzey, S.E. Rogers, O. Shebanova, T. Snow, J.P. Sutter, E.P. Williams, N.J. Terrill, I22: SAXS/WAXS beamline at Diamond Light Source – an overview of 10 years operation, *J. Synchrotron Radiat.* 28 (2021) 939–947, <https://doi.org/10.1107/S1600577521002113>.
- [36] J. Filik, A.W. Ashton, P.C.Y. Chang, P.A. Chater, S.J. Day, M. Drakopoulos, M.W. Gerring, M.L. Hart, O.V. Magdysyuk, S. Michalik, A. Smith, C.C. Tang, N.J. Terrill, M.T. Wharmby, H. Wilhelm, Processing two-dimensional X-ray diffraction and small-angle scattering data in DAWN 2, *J. Appl. Crystallogr.* 50 (2017) 959–966, <https://doi.org/10.1107/S1600576717004708>.
- [37] P.R.O. CrysAlis, O.D. Rigaku, Rigaku Oxford Diffraction Ltd, Yarnton, Oxfordshire, England, 2019.
- [38] L. Palatinus, G. Chapuis, Superflip – a computer program for the solution of crystal structures by charge flipping in arbitrary dimensions, *J. Appl. Crystallogr.* 40 (2007) 786–790, <https://doi.org/10.1107/S0021889807029238>.
- [39] P.W. Betteridge, J.R. Carruthers, R.L. Cooper, K. Prout, D.J. Watkin, CRYSTALS version 12: software for guided crystal structure analysis, *J. Appl. Crystallogr.* 36 (2003) 1487, <https://doi.org/10.1107/S0021889803021800>, 1487.
- [40] W. Harnying, J.M. Neudörfl, A. Berkessel, Enantiospecific synthesis of nepetalactones by one-step oxidative NHC catalysis, *Org. Lett.* 22 (2020) 386–390, <https://doi.org/10.1021/acs.orglett.9b04034>.
- [41] C.E. Ingham, G.C. Hampson, An investigation of steric influences on the phenomenon of resonance. Part II, 209, *J. Chem. Soc.* (1939) 981, <https://doi.org/10.1039/jr9390000981>.
- [42] A.G. Gavriel, F. Leroux, G.S. Khurana, V.G. Lewis, A.M. Chippindale, M.R. Sambrook, W. Hayes, A.T. Russell, Self-immolative system for disclosure of reactive electrophilic alkylating agents: understanding the role of the reporter group, *J. Org. Chem.* 86 (2021) 10263–10279, <https://doi.org/10.1021/acs.joc.1c00996>.
- [43] H.L. Snape, LXXVI.—action of phenyl cyanate on polyhydric and certain monohydric alcohols and phenols, *J. Chem. Soc. Trans.* 47 (1885) 770–779, <https://doi.org/10.1039/CT8854700770>.
- [44] F. Leuthardt, R. Brunner, Réaction entre l'acétyl-acétanilide et les amines primaires, *Helv. Chim. Acta* 30 (1947) 958–964, <https://doi.org/10.1002/hlca.19470300405>.
- [45] A. Michael, P.H. Cobb, Phenylisocyanat als Reagens zur Feststellung der Constitution merotroper Verbindungen, *Justus Liebig's Ann. Der Chemie* 363 (1908) 64–93, <https://doi.org/10.1002/jlac.19083630105>.
- [46] D.J. Beaver, D.P. Roman, P.J. Stoffel, The preparation and bacteriostatic activity of substituted m-nitrocarbanilides, *J. Org. Chem.* 24 (1959) 1676–1678, <https://doi.org/10.1021/jo01093a012>.
- [47] J. Ellena, A.E. Goeta, J.A.K. Howard, G. Punte, Role of the hydrogen bonds in nitroanilines aggregation: charge density study of 2-Methyl-5-nitroaniline, *J. Phys. Chem.* 105 (2001) 8696–8708, <https://doi.org/10.1021/jp010688h>.
- [48] P. Woodward, D.H. Merino, I.W. Hamley, A.T. Slark, W. Hayes, Thermally responsive elastomeric supramolecular polymers featuring flexible Aliphatic hydrogen-bonding end-groups, *Aust. J. Chem.* 62 (2009) 790–793, <https://doi.org/10.1071/CH09088>.
- [49] A. Feula, X. Tang, I. Giannakopoulos, A.M. Chippindale, I.W. Hamley, F. Greco, C. Paul Buckley, C.R. Siviour, W. Hayes, An adhesive elastomeric supramolecular polyurethane healable at body temperature, *Chem. Sci.* 7 (2016) 4291–4300, <https://doi.org/10.1039/c5sc04864h>.
- [50] D. Hermida-Merino, L.R. Hart, P.J. Harris, A.T. Slark, I.W. Hamley, W. Hayes, The effect of chiral end groups on the assembly of supramolecular polyurethanes, *Polym. Chem.* 12 (2021) 4488–4500, <https://doi.org/10.1039/d1py00714a>.
- [51] M. Chen, D.L. Inglefield, K. Zhang, A.G. Hudson, S.J. Talley, R.B. Moore, T.E. Long, Synthesis of urea-containing ABA triblock copolymers: influence of pendant hydrogen bonding on morphology and thermomechanical properties, *J. Polym. Sci. Part A Polym. Chem.* 56 (2018) 1844–1852, <https://doi.org/10.1002/pola.29066>.
- [52] Q. Zhang, C.Y. Shi, D.H. Qu, Y.T. Long, B.L. Feringa, H. Tian, Exploring a naturally tailored small molecule for stretchable, self-healing, and adhesive supramolecular polymers, *Sci. Adv.* 4 (2018) 1–9, <https://doi.org/10.1126/sciadv.aat8192>.
- [53] S. Gao, G. Ma, J. Ye, L. He, L. Guo, X. Li, T. Qiu, X. Tuo, The tough, fluorescent and adhesive elastomer in aqueous dispersion: the contribution of aromatic amide-urea segments, *Mater. Today Commun* 29 (2021), <https://doi.org/10.1016/j.mtcomm.2021.102880>.
- [54] B.C. Baker, A.L. Acton, G.C. Stevens, W. Hayes, Bis amide-aromatic-ureas – highly effective hydro- and organogelator systems, *Tetrahedron* 70 (2014) 8303–8311, <https://doi.org/10.1016/j.tet.2014.09.017>.
- [55] B.C. Baker, C.L. Higgins, D. Ravishankar, H.M. Colquhoun, G.C. Stevens, F. Greco, B.W. Greenland, W. Hayes, Multifunctional, biocompatible, non-peptidic hydrogels: from water purification to drug delivery, *ChemistrySelect* 1 (2016) 1641–1649, <https://doi.org/10.1002/slct.201600249>.
- [56] R.H. Birtles, G.C. Hampson, 3. An investigation of steric influences on the phenomenon of mesomerism, *J. Chem. Soc.* 10 (1937), <https://doi.org/10.1039/jr9370000010>.
- [57] W.P.J. Appel, G. Portale, E. Wisse, P.Y.W. Dankers, E.W. Meijer, Aggregation of ureido-pyrimidinone supramolecular thermoplastic elastomers into nanofibers: a kinetic analysis, *Macromolecules* 44 (2011) 6776–6784, <https://doi.org/10.1021/ma201303s>.
- [58] Y. Chen, A.M. Kushner, G.A. Williams, Z. Guan, Multiphase design of autonomic self-healing thermoplastic elastomers, *Nat. Chem.* 4 (2012) 467–472, <https://doi.org/10.1038/nchem.1314>.
- [59] Y. Lai, X. Kuang, P. Zhu, M. Huang, X. Dong, D. Wang, Colorless, transparent, robust, and fast scratch-self-healing elastomers via a phase-locked dynamic bonds design, *Adv. Mater.* 30 (2018) 1–8, <https://doi.org/10.1002/adma.201802556>.
- [60] D.H. Merino, A. Feula, K. Melia, A.T. Slark, I. Giannakopoulos, C.R. Siviour, C.P. Buckley, B.W. Greenland, D. Liu, Y. Gan, P.J. Harris, A.M. Chippindale, I.W. Hamley, W. Hayes, A systematic study of the effect of the hard end-group composition on the microphase separation, thermal and mechanical properties of supramolecular polyurethanes, *Polymer* 107 (2016) 368–378, <https://doi.org/10.1016/j.polymer.2016.07.029>.
- [61] X. Tang, A. Feula, B.C. Baker, K. Melia, D. Hermida Merino, I.W. Hamley, C.P. Buckley, W. Hayes, C.R. Siviour, A dynamic supramolecular polyurethane network whose mechanical properties are kinetically controlled, *Polymer* 133 (2017) 143–150, <https://doi.org/10.1016/j.polymer.2017.11.005>.
- [62] P.J. Woodward, D.H. Merino, B.W. Greenland, I.W. Hamley, Z. Light, A.T. Slark, W. Hayes, Hydrogen bonded supramolecular elastomers: correlating hydrogen bonding strength with morphology and rheology, *Macromolecules* 43 (2010) 2512–2517, <https://doi.org/10.1021/ma9027646>.
- [63] B.D. Kaushiva, S.R. McCartney, G.R. Rossmly, G.L. Wilkes, Surfactant level influences on structure and properties of flexible slabstock polyurethane foams, *Polymer* 41 (2000) 285–310, [https://doi.org/10.1016/S0032-3861\(99\)00135-4](https://doi.org/10.1016/S0032-3861(99)00135-4).
- [64] S. Sivakova, D.A. Bohnsack, M.E. Mackay, P. Suwanmala, S.J. Rowan, Utilization of a combination of weak hydrogen-bonding interactions and phase segregation to yield highly thermosensitive supramolecular polymers, *J. Am. Chem. Soc.* 127 (2005) 18202–18211, <https://doi.org/10.1021/ja055245w>.
- [65] S. George, A. Nangia, C.K. Lam, T.C.W. Mak, J.F. Nicoud, Crystal engineering of urea  $\alpha$ -network via I...O2N synthon and design of SHG active crystal N-4-iodophenyl-N'-4'-nitrophenylurea, *Chem. Commun.* 4 (2004) 1202–1203, <https://doi.org/10.1039/b402050b>.
- [66] G. Cui, V.A.H. Boudara, Q. Huang, G.P. Baeza, A.J. Wilson, O. Hassager, D.J. Read, J. Mattsson, Linear shear and nonlinear extensional rheology of unentangled supramolecular side-chain polymers, *J. Rheol.* 62 (2018) 1155–1174, <https://doi.org/10.1122/1.5012349>.
- [67] F. Herbst, S. Seiffert, W.H. Binder, Dynamic supramolecular poly(isobutylene)s for self-healing materials, *Polym. Chem.* 3 (2012) 3084–3092, <https://doi.org/10.1039/c2py20265d>.

- [68] L.N. Neumann, E. Oveisi, A. Petzold, R.W. Style, T. Thurn-Albrecht, C. Weder, S. Schrettl, Dynamics and healing behavior of metallosupramolecular polymers, *Sci. Adv.* 7 (2021) 1–9, <https://doi.org/10.1126/sciadv.abe4154>.
- [69] J.L. Dalsin, B.H. Hu, B.P. Lee, P.B. Messersmith, Mussel adhesive protein mimetic polymers for the preparation of nonfouling surfaces, *J. Am. Chem. Soc.* 125 (2003) 4253–4258, <https://doi.org/10.1021/ja0284963>.
- [70] C.E. Brubaker, P.B. Messersmith, The present and future of biologically inspired adhesive interfaces and materials, *Langmuir* 28 (2012) 2200–2205, <https://doi.org/10.1021/la300044v>.
- [71] D.W.R. Balkenende, C.A. Monnier, G.L. Fiore, C. Weder, Optically responsive supramolecular polymer glasses, *Nat. Commun.* 7 (2016) 1–9, <https://doi.org/10.1038/ncomms10995>.
- [72] G. Raos, B. Zappone, Polymer adhesion: seeking new solutions for an old problem, *Macromolecules* 54 (2021) 10617–10644, <https://doi.org/10.1021/acs.macromol.1c01182>.
- [73] S. Salimi, L.R. Hart, A. Feula, D. Hermida-Merino, A.B.R. Touré, E.A. Kabova, L. Ruiz-Cantu, D.J. Irvine, R. Wildman, K. Shankland, W. Hayes, Property enhancement of healable supramolecular polyurethanes, *Eur. Polym. J.* 118 (2019) 88–96, <https://doi.org/10.1016/j.eurpolymj.2019.05.042>.
- [74] D. Döhler, J. Kang, C.B. Cooper, J.B.H. Tok, H. Rupp, W.H. Binder, Z. Bao, Tuning the self-healing response of poly(dimethylsiloxane)-based elastomers, *ACS Appl. Polym. Mater.* 2 (2020) 4127–4139, <https://doi.org/10.1021/acscapm.0c00755>.